

1 **Millennial-scale variations of sedimentary oxygenation in the western**
2 **subtropical North Pacific and its links to North Atlantic climate**

3
4 Jianjun Zou^{1,2}, Xuefa Shi^{1,2}, Aimei Zhu¹, Selvaraj Kandasamy³, Xun Gong⁴, Lester
5 Lembke-Jene⁴, Min-Te Chen⁵, Yonghua Wu^{1,2}, Shulan Ge^{1,2}, Yanguang Liu^{1,2}, Xinru
6 Xue¹, Gerrit Lohmann⁴, Ralf Tiedemann⁴

7 ¹Key Laboratory of Marine Sedimentology and Environmental Geology, First Institute
8 of Oceanography, MNR, Qingdao 266061, China

9 ²Laboratory for Marine Geology, Qingdao National Laboratory for Marine Science
10 and Technology, Qingdao, 266061, China

11 ³Department of Geological Oceanography and State Key Laboratory of Marine
12 Environmental Science, Xiamen University, Xiamen361102, China

13 ⁴Alfred-Wegener-Institut Helmholtz-Zentrum für Polar- und Meeresforschung, Am
14 Handelshafen 12, 27570 Bremerhaven, Germany

15 ⁵Institute of Applied Geosciences, National Taiwan Ocean University, Keelung 20224,
16 Taiwan

17
18 Corresponding authors:

19 Jianjun Zou (zoujianjun@fio.org.cn); Xuefa Shi (xfshi@fio.org.cn)

20 **Key Points**

21 1. This study reconstructs the history of sedimentary oxygenation processes at
22 mid-depths in the western subtropical North Pacific since the last glacial period.

23 2. Sediment-bound redox-sensitive proxies reveal millennial-scale variations in
24 sedimentary oxygenation that correlated closely to changes in the North Pacific
25 Intermediate Water.

26 3. A millennial-scale out-of-phase relationship between deglacial ventilation in the
27 western subtropical North Pacific and the formation of North Atlantic Deep Water is
28 suggested.

29 4. A larger CO₂ storage at mid-depths of the North Pacific corresponds to the
30 termination of atmospheric CO₂ rise during the Bölling-Alleröd interval.

31 **Abstract**

32 The deep ocean carbon cycle, especially carbon sequestration and outgassing, is
33 one of the mechanisms to explain variations in atmospheric CO₂ concentrations on
34 millennial and orbital timescales. However, the potential role of subtropical North
35 Pacific subsurface waters in modulating atmospheric CO₂ levels on millennial
36 timescales is poorly constrained. An increase in respired CO₂ concentration in the
37 glacial deep ocean due to biological pump generally corresponds to deoxygenation in
38 the ocean interior. This link thus offers a chance to study oceanic ventilation and
39 coeval export productivity based on redox-controlled, sedimentary geochemical
40 parameters. Here, we investigate a suite of geochemical proxies in a sediment core
41 from the Okinawa Trough to understand sedimentary oxygenation variations in the
42 subtropical North Pacific over the last 50,000 years (50 ka). Our results suggest that
43 enhanced mid-depth western subtropical North Pacific (WSTNP) sedimentary
44 oxygenation occurred during cold intervals and after 8.5 ka, while oxygenation
45 decreased during the Bölling-Alleröd (B/A) and Preboreal. The enhanced oxygenation
46 during cold spells is linked to the North Pacific Intermediate Water (NPIW), while
47 interglacial increase after 8.5 ka is linked to an intensification of the Kuroshio Current
48 due to strengthened northeast trade winds over the tropics. The enhanced formation of
49 NPIW during Heinrich Stadial 1 (HS1) was likely driven by the perturbation of sea
50 ice formation and sea surface salinity oscillations in high-latitude North Pacific. The
51 diminished sedimentary oxygenation during the B/A due to decreased NPIW
52 formation and enhanced export production, indicates an expansion of oxygen
53 minimum zone in the North Pacific and enhanced CO₂ sequestration at mid-depth
54 waters, along with termination of atmospheric CO₂ concentration increase. We
55 attribute the millennial-scale changes to intensified NPIW and enhanced abyss
56 flushing during deglacial cold and warm intervals, respectively, closely related to
57 variations in North Atlantic Deep Water formation.

58 **Keywords:** sedimentary oxygenation; millennial timescale; North Pacific
59 Intermediate Water; North Atlantic Deep Water; subtropical North Pacific

60 **1. Introduction**

61 A more sluggish deep ocean ventilation combined with a more efficient
62 biological pump is widely thought to facilitate enhanced carbon sequestration in the
63 ocean interior, leading to atmospheric CO₂ drawdown during glacial cold periods
64 (Sigman and Boyle, 2000). These changes are tightly coupled to bottom water
65 oxygenation and sedimentary redox changes on both millennial and orbital timescales
66 (Hoogakker et al., 2015; Jaccard and Galbraith, 2012; Sigman and Boyle, 2000).
67 Reconstruction of past sedimentary oxygenation is therefore crucial for understanding
68 changes in export productivity and renewal of deep ocean circulation (Nameroff et al.,
69 2004). Previous studies from North Pacific margins as well as open subarctic Pacific
70 have identified drastic variations in export productivity and ocean oxygen levels at
71 millennial and orbital timescales using diverse proxies such as trace elements
72 (Cartapanis et al., 2011; Chang et al., 2014; Jaccard et al., 2009; Zou et al., 2012),
73 benthic foraminiferal assemblages (Ohkushi et al., 2016; Ohkushi et al., 2013;
74 Shibahara et al., 2007) and nitrogen isotopic composition ($\delta^{15}\text{N}$) of organic matter
75 (Addison et al., 2012; Chang et al., 2014; Galbraith et al., 2004; Riethdorf et al., 2016)
76 in marine sediment cores. These studies suggested that both North Pacific
77 Intermediate Water (NPIW) and export of organic matter regulate the sedimentary
78 oxygenation variation during the last glaciation and Holocene in the subarctic Pacific.
79 By contrast, little information exists on millennial-scale oxygenation changes to date
80 in the western subtropical North Pacific (WSTNP).

81 The modern NPIW precursor waters are mainly sourced from the NW Pacific
82 marginal seas (Shcherbina et al., 2003; Talley, 1993; You et al., 2000), spreading into
83 the subtropical North Pacific at intermediate depths of 300 to 800 m (Talley, 1993).
84 The pathway and circulation of NPIW have been identified by You (2003), who
85 suggested that cabbeling, a mixing process to form a new water mass with increased
86 density than that of parent water masses, is the principle mechanism responsible for
87 transforming subpolar source waters into subtropical NPIW along the
88 subarctic-tropical frontal zone. More specifically, a small subpolar input of about 2 Sv
89 ($1 \text{ Sv} = 10^6 \text{ m}^3/\text{s}$) is sufficient for subtropical ventilation (You et al., 2003). Benthic

90 foraminiferal $\delta^{13}\text{C}$, a quasi-conservative tracer for water mass, from the North Pacific
91 indicates an enhanced ventilation (higher $\delta^{13}\text{C}$) at water depths of < 2000 m during
92 the last glacial period (Keigwin, 1998; Matsumoto et al., 2002). Furthermore, on the
93 basis of both radiocarbon data and modeling results, Okazaki et al. (2010) suggested
94 the formation of deep water in the North Pacific during the early deglaciation in
95 Heinrich Stadial 1 (HS1). Enhanced NPIW penetration was further explored using
96 numerical model simulations (Chikamoto et al., 2012; Gong et al., 2019; Okazaki et
97 al., 2010). In contrast, substantial effects of intensified NPIW formation during
98 Marine Isotope Stage (MIS) 2 and 6 on the ventilation and nutrient characteristics of
99 lower latitude mid-depth Eastern Equatorial Pacific have been suggested by recent
100 studies (Max et al., 2017; Rippert et al., 2017). The downstream effects of intensified
101 NPIW are also reflected in the record of $\delta^{13}\text{C}$ of *Cibicides wuellerstorfi* in core PN-3
102 from the middle Okinawa Trough (OT), where lower deglacial $\delta^{13}\text{C}$ values were
103 attributed to enhanced OC accumulation rates due to higher surface productivity by
104 (Wahyudi and Minagawa, 1997).

105 The Okinawa Trough is separated from the Philippine Sea by the Ryukyu Islands
106 and is an important channel of the northern extension of the Kuroshio in the WSTNP
107 (Figure 1). Initially the OT opened at the middle Miocene (Sibuet et al., 1987) and
108 since then, it has been a depositional center in the East China Sea (ECS), receiving
109 large sediment supplies from nearby rivers (Chang et al., 2009). Surface
110 oceanographic characteristics of the OT over glacial-interglacial cycles are largely
111 influenced by the Kuroshio and ECS Coastal Water (Shi et al., 2014); the latter is
112 related to the strength of summer East Asian monsoon (EAM) sourced from the
113 western tropical Pacific. Modern physical oceanographic investigations showed that
114 intermediate waters in the OT are mainly derived from horizontal advection and
115 mixing of NPIW and South China Sea Intermediate Water (Nakamura et al., 2013).
116 These waters intrude into the OT through two ways: (i) deeper part of the Kuroshio
117 enters the OT through the channel east of Taiwan (sill depth 775 m) and (ii) through
118 the Kerama Gap (sill depth 1100 m). In the northern OT, the subsurface water mainly
119 flows through horizontal advection through the Kerama Gap from the Philippine Sea

120 (Nakamura et al., 2013). Recently, Nishina et al. (2016) found that an overflow
121 through the Kerama Gap controls the modern deep-water ventilation in the southern
122 OT.

123 Both surface characteristics and deep ventilation in the OT varied significantly
124 since the last glaciation. During the last glacial period, the mainstream of the
125 Kuroshio likely migrated to the east of the Ryukyu Islands or also became weaker due
126 to lower sea levels (Shi et al., 2014; Ujiie and Ujiie, 1999; Ujiie et al., 2003) and the
127 hypothetical emergence of a Ryukyu-Taiwan land bridge (Ujiie and Ujiie, 1999). In a
128 recent study, based on the Mg/Ca-derived temperatures in surface and thermocline
129 waters, and planktic foraminiferal indicators of water masses from two sediment cores
130 located in the northern and southern OT, Ujiie et al. (2016) argued that the
131 hydrological conditions of the North Pacific Subtropical Gyre since MIS 7 is
132 modulated by the interaction between the Kuroshio and the NPIW. Besides the
133 Kuroshio, the flux of East Asian rivers to the ECS, which is related to the summer
134 EAM and the sea level oscillations coupled with topography have also been regulating
135 the surface hydrography in the OT (Chang et al., 2009; Kubota et al., 2010; Sun et al.,
136 2005; Yu et al., 2009).

137 Based on benthic foraminiferal assemblages, previous studies have implied a
138 reduced oxygenation in deep waters of the middle and southern OT during the last
139 deglacial period (Jian et al., 1996; Li et al., 2005), but a strong ventilation during the
140 Last Glacial Maximum (LGM) and the Holocene (Jian et al., 1996; Kao et al., 2005).
141 High sedimentary $\delta^{15}\text{N}$ values, an indicator of increased denitrification in the
142 subsurface water column, also occurred during the late deglaciation in the middle OT
143 (Kao et al., 2008). Inconsistent with these results, Dou et al. (2015) suggested an oxic
144 depositional environment during the last deglaciation in the southern OT based on
145 weak positive cerium anomalies. Furthermore, Kao et al. (2006) hypothesized a
146 reduced ventilation of deepwater in the OT during the LGM due to the reduction of
147 KC inflow using a 3-D ocean model. Thus, the patterns and reasons that caused
148 sedimentary oxygenation in the OT remain controversial.

149 **2. Paleo-redox proxies**

150 The sedimentary redox conditions are governed by the rate of oxygen supply from
151 the overlying bottom water and the rate of oxygen removal from pore water (Jaccard
152 et al., 2016), processes that are related to the supply of oxygen by ocean circulation
153 and organic matter respiration, respectively. Contrasting geochemical behaviors of
154 redox-sensitive trace metals (Mn, Mo, U, etc.) have been used to reconstruct bottom
155 water and sedimentary oxygen changes (Algeo, 2004; Algeo and Lyons, 2006;
156 Crusius et al., 1996; Dean et al., 1997; Tribovillard et al., 2006; Zou et al., 2012), as
157 their concentrations readily respond to redox condition of the depositional
158 environment (Morford and Emerson, 1999).

159 In general, enrichment of Mn with higher speciation states (Mn (III) and Mn (IV))
160 in the form of Mn-oxide coatings is observed in marine sediments, when oxic
161 conditions prevail into greater sediment depths as a result of low organic matter
162 degradation rates and well-ventilated bottom water (Burdige, 1993). Under reducing
163 conditions, the authigenic fraction of Mn (as opposed to its detrital background) is
164 released as dissolved Mn (II) species into the pore water and thus its concentration is
165 usually low in suboxic (O_2 and HS^- absent) and anoxic (HS^- present) sediments. In
166 addition, when Mn enrichment occurs in oxic sediments as solid phase Mn
167 oxyhydroxides, it may lead to co-precipitation of other elements, such as Mo
168 (Nameroff et al., 2002).

169 The elements Mo and U behave conservatively in oxygenated seawater, but are
170 preferentially enriched in oxygen-depleted water (Morford and Emerson, 1999).
171 However, these two trace metals behave differently in several ways. Molybdenum can
172 be enriched in both oxic sediments, such as the near surface manganese-rich horizons
173 in continental margin environments (Shimmield and Price, 1986) and in anoxic
174 sediments (Nameroff et al., 2002). Under anoxic conditions, Mo can be reduced either
175 from the +6 oxidation state to insoluble MoS_2 , though this process is known to occur
176 only under extremely reducing conditions, such as hydrothermal and/or diagenesis
177 (Dahl et al., 2010; Helz et al., 1996) or be converted to particle-reactive
178 thiomolybdates (Vorlicek and Helz, 2002). Zheng et al. (2000) suggested two critical
179 thresholds for Mo scavenging from seawater: 0.1 μM hydrogen sulfide (H_2S) for

180 Fe-S-Mo co-precipitation and 100 μM H_2S for Mo scavenging as Mo-S or as
181 particle-bound Mo without Fe. Although Crusius et al. (1996) noted insignificant
182 enrichment of sedimentary Mo under suboxic conditions, Scott et al. (2008) argued
183 that burial flux of Mo is not so low in suboxic environments. Excess concentration of
184 Mo ($\text{Mo}_{\text{excess}}$) in sediments thus suggests the accumulation of sediments either in
185 anoxic (H_2S occurrence) or well oxygenated conditions (if $\text{Mo}_{\text{excess}}$ is in association
186 with Mn-oxides).

187 In general, U is enriched in anoxic sediments ($>1 \mu\text{M}$ H_2S), but not in oxic
188 sediments ($>10 \mu\text{M}$ O_2) (Nameroff et al., 2002). Accumulation of U depends on the
189 content of reactive organic matter (Sundby et al., 2004) and U precipitates as uraninite
190 (UO_2) during the conversion of Fe (III) to Fe (II) in suboxic conditions (Morford and
191 Emerson, 1999; Zheng et al., 2002). One of the primary removal mechanisms for U
192 from the ocean is via diffusion across the sediment-water interface of reducing
193 sediments (Klinkhammer and Palmer, 1991). Under suboxic conditions, soluble U (VI)
194 is reduced to insoluble U (IV), but free sulfide is not required for U precipitation
195 (McManus et al., 2005). Jaccard et al. (2009) suggested that the presence of excess
196 concentration of U (U_{excess}) in the absence of Mo enrichment is indicative of a suboxic,
197 but not sulfidic condition, within the diffusional range of the sediment-water interface.
198 The felsic volcanism is also a primary source of uranium (Maithani and Srinivasan,
199 2011). Therefore, the potential input of uranium from active volcanic sources around
200 the northwestern Pacific to the adjacent sediments should not be neglected.

201 In this study, we investigate a suite of redox-sensitive elements and the ratio of
202 Mo/Mn along with productivity proxies from a sediment core retrieved from the
203 northern OT to reconstruct the sedimentary oxygenation in the WSTNP over the last
204 50ka. Based on that, we propose that multiple factors, such as NPIW ventilation, the
205 strength of the Kuroshio Current and export productivity, control the bottom
206 sedimentary oxygenation in the OT on millennial timescales since the last glacial.

207 **3. Oceanographic setting**

208 Surface hydrographic characteristics of the OT are mainly controlled by the
209 warmer, more saline, oligotrophic Kuroshio water and cooler, less saline, nutrient-rich

210 Changjiang Diluted Water, and the modern flow-path of the former is influenced by
211 the bathymetry of the OT (Figure 1a). The Kuroshio Current originates from the
212 North Equatorial Current and flows into the ECS from the Philippine Sea through the
213 Suao-Yonaguni Depression. In the northern OT, Tsushima Warm Current (TWC), a
214 branch of the Kuroshio, flows into the Japan Sea through the shallow Tsushima Strait.
215 Volume transport of the Kuroshio varies seasonally due to the influence of the EAM
216 with a maximum of 24 Sv in summer and a minimum of 20 Sv in autumn across the
217 east of Taiwan (Qu and Lukas, 2003).

218 A lower sea surface salinity (SSS) zone in summer relative to the one in winter in
219 the ECS migrates toward the east of OT, indicating enhanced impact of the
220 Changjiang discharge associated with summer EAM (Figures 2a and 2b). An
221 estimated ~80% of the mean annual discharge of the river Changjiang is supplied to
222 the ECS (Ichikawa and Beardsley, 2002) and in situ observational data show a
223 pronounced negative correlation between the Changjiang discharge and SSS in July
224 (Delcroix and Murtugudde, 2002). Consistently, previous studies from the OT
225 reported such close relationship between summer EAM and SSS back to the late
226 Pleistocene (Chang et al., 2009; Clemens et al., 2018; Kubota et al., 2010; Sun et al.,
227 2005).

228 Despite the effects of EAM and the Kuroshio, evidence of geochemical tracers
229 (temperature, salinity, oxygen, nutrients and radiocarbon) collected during the World
230 Ocean Circulation Experiment (WOCE) in the Pacific (transects P24 and P03) favors
231 the presence of low salinity, nutrient-enriched intermediate and deep waters (Talley,
232 2007). Dissolved oxygen content is <100 $\mu\text{mol/kg}$ at water depths below 600 m in the
233 OT, along WOCE transects PC03 and PC24 (Talley, 2007). Modern oceanographic
234 observations at the Kerama Gap reveal that upwelling in the OT is associated with the
235 inflow of NPIW and studies using a box model predicted that overflow through the
236 Kerama Gap is responsible for upwelling ($3.8\text{--}7.6 \times 10^{-6} \text{m s}^{-1}$) (Nakamura et al.,
237 2013; Nishina et al., 2016).

238 **4. Materials and methods**

239 **4.1. Chronostratigraphy of core CSH1**

240 A 17.3 m long sediment core CSH1 (31° 13.7' N, 128° 43.4' E; water depth: 703
241 m) was collected from the northern OT, close to the main stream of Tsushima Warm
242 Current (TWC) (Figure 1b) and within the depth of NPIW (Figure 1c) using a piston
243 corer during *Xiangyanghong09* Cruise in 1998, carried out by the First Institute of
244 Oceanography, Ministry of Natural Resources of China. This location is enabling us
245 to reconstruct millennial-scale changes in the properties of TWC and NPIW. Core
246 CSH1 mainly consists of clayey silt and silt with occurrence of plant debris at some
247 depth intervals (Ge et al., 2007) (Figure 3a). In addition, three layers of volcanic ash
248 were observed at depths of 74–106 cm, 782–794 cm, 1570–1602 cm. These three
249 intervals can be correlated with well-known ash layers, Kikai-Akahoya (K-Ah; 7.3
250 ka), Aira-Tanzawa (AT; 29.24 ka) and Aso-4 (roughly around MIS 5a) (Machida,
251 1999), respectively. The core was split and sub-sampled at 4 cm interval and then
252 stored in the China Ocean Sample Repository at 4 °C until analysis.

253 Previously, paleoceanographic studies have been conducted and a set of data has
254 been investigated for core CSH1, including the contents of planktic foraminifers as
255 well as their carbon ($\delta^{13}\text{C}$) and oxygen isotope ($\delta^{18}\text{O}$) compositions (Shi et al., 2014),
256 pollen (Chen et al., 2006), paleomagnetism (Ge et al., 2007) and CaCO_3 (Wu et al.,
257 2004). An age model for this core has been constructed by using ten Accelerator Mass
258 Spectrometry (AMS) ^{14}C dates and six oxygen isotope ($\delta^{18}\text{O}$) age control points. The
259 whole 17.3 m core contains *ca.* 88 ka-long record of continuous sedimentation (Shi et
260 al., 2014).

261 Notably, the original age model, which used constant radiocarbon reservoir ages
262 throughout core CSH1 are suitable to reveal orbital-scale Kuroshio variations (Shi et
263 al., 2014), but insufficient to investigate millennial-scale climatic events. A higher
264 abundance of *Neogloboquadrina pachyderma (dextral)*, e. g. that occurred during
265 warmer intervals, such as the Bölling-Alleröd (B/A), has been challenging to explain.
266 On the other hand, paired measurements of $^{14}\text{C}/^{12}\text{C}$ and ^{230}Th ages from Hulu Cave
267 stalagmites suggest magnetic field changes have greatly contributed to high
268 atmospheric $^{14}\text{C}/^{12}\text{C}$ values at HS4 and the Younger Dryas (YD) (Cheng et al., 2018).
269 Thus a constant reservoir age ($\Delta R=0$) assumed when calibrating foraminiferal

270 radiocarbon dates using CALIB 6 software and the Marine 13 calibration dataset
271 (Reimer et al., 2013) for core CSH1 may cause large chronological uncertainties.

272 Here, we recalibrated the radiocarbon dates using updated CALIB 7.04 software
273 with Marine 13 calibration dataset (Reimer et al., 2013). Moreover, on the basis of
274 significant correlation between planktic foraminifera species *Globigerinoides ruber*
275 $\delta^{18}\text{O}$ and Chinese stalagmite $\delta^{18}\text{O}$ (Cheng et al., 2016), a proxy of summer EAM
276 related to SSS of the ECS, we improve the age model for core CSH1 (Figures 3b-3d).
277 Overall, the new chronological framework is similar to the one previously reported by
278 Shi et al. (2014), but with more dates. In order to compare with published results
279 associated with ventilation changes in the North Pacific, here we mainly report the
280 history of sedimentary oxygenation in the northern OT since the last glacial period.
281 Linear sedimentation rate varied between ~ 10 and 40 cm/ka with higher
282 sedimentation rates (around $30\text{-}40$ cm/ka) between ~ 24 ka and 32.5 ka. Variation in
283 sedimentation rate has been attributed to changes in eustatic sea level, summer EAM
284 intensity, path and/or intensity of Kuroshio Current. Generally, sea level is thought to
285 be the first-order factor for controlling linear sedimentation rate changes (Beny et al.,
286 2018; Li et al., 2015; Zhao et al., 2017). The new age control points are shown in
287 Table 2.

288 **4.2. Chemical analyses**

289 Sediment subsamples for geochemical analyses were freeze-dried and ground to
290 a fine powder with an agate mortar and pestle. Based on the age model, 85
291 subsamples from core CSH1, representing a temporal resolution of about 600 years
292 (every 4 cm interval) were selected for detailed geochemical analyses of major and
293 minor elements, and total carbon (TC), organic carbon (TOC) and nitrogen (TN)
294 contents. The pretreatment of sediment and other analytical methods have been
295 reported elsewhere (Zou et al., 2012).

296 TC and TN were determined with an elemental analyzer (EA; Vario EL III,
297 Elementar Analysen systeme GmbH) in the Key Laboratory of Marine Sediment and
298 Environment Geology, First Institute of Oceanography, Ministry of Natural Resources
299 of China, Qingdao. Carbonate was removed from sediments by adding 1M HCl to the

300 homogenized sediments for total organic carbon (TOC) analysis using the same
301 equipment. The content of calcium carbonate (CaCO₃) was calculated using the
302 equation:

$$303 \quad \text{CaCO}_3 = (\text{TC} - \text{TOC}) \times 8.33$$

304 where 8.33 is the ratio between the molecular weight of carbonate and the atomic
305 weight of carbon. National reference material (GSD-9), blank sample and replicated
306 samples were used to control the analytical process. The relative standard deviation of
307 the GSD-9 for TC, TN and TOC is $\leq 3.4\%$.

308 About 0.5 g of sediment powder was digested in double distilled HF:HNO₃ (3:1),
309 followed by concentrated HClO₄, and then re-dissolved in 5% HNO₃. Selected major
310 and minor elements such as aluminum (Al) and manganese (Mn) were determined by
311 inductively coupled plasma optical emission spectroscopy (ICP-OES; Thermo
312 Scientific iCAP 6000, Thermo Fisher Scientific), as detailed elsewhere (Zou et al.,
313 2012). In addition, Mo and U were analyzed with inductively coupled plasma mass
314 spectrometry (ICP-MS; Thermo Scientific XSERIES 2, Thermo Fisher Scientific), as
315 described in Zou et al. (2012). Precision for most elements in the reference material
316 GSD-9 is $\leq 5\%$ relative standard deviation. The excess fractions of U and Mo were
317 estimated by normalization to Al:

$$318 \quad \text{Excess fraction} = \frac{\text{total}_{\text{element}}}{\text{Al}_{\text{average shale}}} - \left(\frac{\text{element}}{\text{Al}_{\text{average shale}}} \times \text{Al} \right), \text{ with } \text{U}/\text{Al}_{\text{average shale}} =$$

319 0.307×10^{-6} and $\text{Mo}/\text{Al}_{\text{average shale}} = 0.295 \times 10^{-6}$ (Li and Schoonmaker, 2014).

320 In addition, given the different geochemical behaviors of Mn and Mo and
321 co-precipitation and adsorption processes associated with the redox cycling of Mn, we
322 calculated the ratio of Mo to Mn, assuming that higher Mo/Mn ratio indicates lower
323 oxygen content in the depositional environment and vice versa. In combination with
324 the concentration of excess uranium, we infer the history of sedimentary oxygenation
325 in the subtropical North Pacific since the last glaciation.

326 **5. Results**

327 **5.1. TOC, TN, and CaCO₃**

328 The content of CaCO₃ varies from 8.8 to 35% (Figure 4a) and it mostly shows
329 higher values with increasing trends during the last deglaciation. In contrast, the

330 content of CaCO₃ is low and exhibits decreasing trends during the late MIS 3 and the
331 LGM (Figure 4a). TN content shows a larger variation compared to TOC (Figure 4b),
332 but it still strongly correlates with TOC ($r = 0.74$, $p < 0.01$) throughout the entire core.
333 Concentration of TOC ranges from 0.5 to 2.1% and it shows higher values with stable
334 trends during the last glacial phase (MIS 3) (Figure 4c). Molar ratios of TOC/TN vary
335 around 10, with higher ratios at the transition into the LGM (Figure 4d),
336 corresponding to higher linear sedimentation rate (Figure 4e).

337 Both TOC and CaCO₃ have been used as proxies for the reconstruction of past
338 export productivity (Cartapanis et al., 2011; Lembke-Jene et al., 2017; Rühlemann et
339 al., 1999). Molar C/N ratios of >10 (Figure 4c) suggest that terrigenous organic
340 sources significantly contribute to the TOC concentration in core CSH1. The TOC
341 content therefore may be not a reliable proxy for the reconstruction of surface water
342 export productivity during times of the LGM and late deglaciation, when maxima in
343 C/N ratios co-occur with decoupled trends between CaCO₃ and TOC concentrations.

344 Several lines of evidence support CaCO₃ as a reliable productivity proxy,
345 particularly during the last deglaciation. The strong negative correlation coefficient (r
346 = -0.85 , $p < 0.01$) between Al and CaCO₃ in sediments throughout core CSH1
347 confirms the biogenic origin of CaCO₃ against terrigenous Al (Figure 4f). Generally,
348 terrigenous dilution decreases the concentrations of CaCO₃. An inconsistent
349 relationship between CaCO₃ contents and sedimentation rates indicates a minor effect
350 of dilution on CaCO₃. Furthermore, the increasing trend in CaCO₃ associated with
351 high sedimentation rate during the last deglacial interval indicates a substantial
352 increase in export productivity (Figures 4a and 4d). The high coherence between
353 CaCO₃ content and alkenone-derived sea surface water (SST) (Shi et al., 2014)
354 indicates a direct control on CaCO₃ by SST. Moreover, a detailed comparison between
355 CaCO₃ concentrations and the previously published foraminiferal fragmentation ratio
356 (Wu et al., 2004) shows, apart from a small portion within the LGM, no clear
357 co-variation between them. These pieces of evidence suggest that CaCO₃ changes are
358 driven primarily by variations in carbonate primary production, and not overprinted
359 by secondary processes, such as carbonate dissolution through changes in the

360 lysocline depth and dilution by terrigenous materials. Likewise, a similar deglacial
361 trend in CaCO_3 is also observed in core MD01-2404 (Chang et al., 2009), indicating a
362 ubiquitous, not local picture in the OT. All these lines of evidence thus support CaCO_3
363 of core CSH1 as a reliable productivity proxy to a first order approximation.

364 **5.2. Redox-sensitive Elements**

365 Figure 4 shows time series of selected redox-sensitive elements (RSEs) and
366 proxies derived from them. Mn shows higher concentrations during the LGM and
367 HS1 (16 ka–22 ka) and middle-late Holocene, but lower concentrations during the last
368 deglacial and Preboreal periods (15.8 ka–9.5 ka, Figure 4g). Generally, concentrations
369 of excess Mo and excess U (Figures 4j and 4l) show coherent patterns with those of
370 Mo and U (Figures 4i and 4k), but both are out-of-phase with Mn over the last glacial
371 period (Figure 4h). Pronounced variations in U concentration after 8.5 ka are related
372 to the occurrence of discrete volcanic materials. A significant positive Eu anomaly
373 (Zhu et al., 2015) confirms the occurrence of discrete volcanic materials and its
374 dilution effects on terrigenous components since 7 ka. Occurrence of discrete volcanic
375 material is likely related to intensified Kuroshio Current during the mid-late Holocene,
376 as supported by higher hydrothermal Hg concentrations in sediments from the middle
377 OT (Lim et al., 2017). A negative correlation between Mn and $\text{Mo}_{\text{excess}}$ during the last
378 glaciation and the Holocene, and the strong positive correlation between them during
379 the LGM and HS1 (Figures 5a and 5b) further corroborate the complex geochemical
380 behaviors of Mn and Mo. A strong positive correlation between $\text{Mo}_{\text{excess}}$ and Mn
381 (Figure 5b) may be attributed to co-precipitation of Mo by Mn-oxyhydroxide under
382 oxygenated conditions. Here, we thus use the Mo/Mn ratio, instead of excess Mo
383 concentration to reconstruct variations in sedimentary redox conditions in our study
384 area. Overall, the Mo/Mn ratio shows similar downcore pattern to that of $\text{Mo}_{\text{excess}}$ with
385 higher ratios during the last deglaciation, but lower ratios during the LGM and HS1. A
386 strong correlation ($r = 0.69$) between Mo/Mn ratio and excess U concentration
387 (excluding the data of Holocene, due to the contamination with volcanic material,
388 Figure 5c) further corroborates the integrity of Mo/Mn as an indicator of sedimentary
389 oxygenation changes.

390 Rapidly decreasing Mo/Mn ratios indicate a well oxygenated sedimentary
391 environment after ~8 ka (Figure 4h). Both higher Mo/Mn ratios and excess U
392 concentrations, together with lower Mn concentrations suggest suboxic depositional
393 conditions during the late deglacial period (15.8 ka–9.5 ka), whereas lower ratios
394 during the LGM, HS1 and HS2 indicate relatively better oxygenated sedimentary
395 conditions. A decreasing trend in Mo/Mn ratio and excess U concentration from 50 ka
396 to 25 ka also suggest higher sedimentary oxygen levels.

397 **6. Discussion**

398 **6.1. Constraining paleoredox conditions in the Okinawa Trough**

399 In general, three different terms, hypoxia, suboxia and anoxia, are widely used to
400 describe the degree of oxygen depletion in the marine environment (Hofmann et al.,
401 2011). Here, we adopt the definition of oxygen thresholds by Bianchi et al. (2012) for
402 oxic ($>120 \mu\text{mol/kg O}_2$), hypoxic ($<60\text{--}120 \mu\text{mol/kg O}_2$) and suboxic ($<2\text{--}10$
403 $\mu\text{mol/kg O}_2$) conditions, whereas anoxia is the absence of measurable oxygen.

404 Proxies associated with RSEs, such as sedimentary Mo concentration (Lyons et
405 al., 2009; Scott et al., 2008) have been used to constrain the degree of oxygenation in
406 seawater. Algeo and Tribovillard (2009) proposed that open-ocean systems with
407 suboxic waters tend to yield U_{excess} enrichment relative to Mo_{excess} , resulting in
408 sediment $(Mo/U)_{\text{excess}}$ ratio less than that of seawater (7.5–7.9). Under increasingly
409 reducing and occasionally sulfidic conditions, the accumulation of Mo_{excess} increase
410 relative to that of U_{excess} leading the $(Mo/U)_{\text{excess}}$ ratio either is equal to or exceeds
411 with that of seawater. Furthermore, Scott and Lyons (2012) suggested a non-euxinic
412 condition with the presence of sulfide in pore waters, when Mo concentrations range
413 from $> 2 \mu\text{g/g}$, the crustal average to $< 25 \mu\text{g/g}$, a threshold concentration for euxinic
414 condition. Given that the northern OT is located in an open oceanic setting, we use
415 these two proxies to evaluate the degree of oxygenation in sediments.

416 Both bulk Mo concentration (1.2–9.5 $\mu\text{g/g}$) and excess (Mo/U) ratio (0.2–5.7) in
417 core CSH1 suggest that oxygen-depleted conditions have prevailed in the deep water
418 of the northern OT over the last 50 ka (Figure 4m). However, increased excess Mo
419 concentrations with higher Mo/U ratios during the last termination (18 ka–9 ka)

420 indicate more reducing conditions compared to the Holocene and the last glacial
421 period, though Mo concentrations were less than 25 µg/g, a threshold for euxinic
422 deposition proposed by Scott and Lyons (2012).

423 The relative abundance of benthic foraminifera species that thrive in different
424 oxygen concentrations has also been widely used to reconstruct variations in bottom
425 water ventilation, such as the enhanced abundance of *Bulimina aculeata*, *Uvigerina*
426 *peregrina* and *Chilostomella oolina* found under oxygen-depleted conditions in the
427 central and southern OT from 18 ka to 9.2 ka (Jian et al., 1996; Li et al., 2005). An
428 oxygenated bottom water condition is also indicated by abundant benthic foraminifera
429 species *Cibicidoides hyalina* and *Globocassidulina subglobosa* after 9.2 ka (Jian et al.,
430 1996; Li et al., 2005) in cores E017 (1826 m water depth) and 255 (1575 m water
431 depth) and high benthic $\delta^{13}\text{C}$ values (Wahyudi and Minagawa, 1997) in core PN-3
432 (1058 m water depth) from the middle and southern OT during the postglacial period.
433 The poorly-ventilated deep water in the middle and southern OT inferred by benthic
434 foraminiferal assemblages during the last deglaciation correlates with the one in the
435 northern OT referring to our RSEs (Figure 4). A link thus can be hypothesized
436 between deep-water ventilation and sedimentary oxygenation in the OT. Overall, a
437 combination of our proxy records of RSEs in core CSH1 with other records shows
438 oxygen-rich conditions during the last glaciation and middle and late Holocene (since
439 8.5 ka) intervals, but oxygen-poor conditions during the last deglaciation.

440 **6.2. Causes for sedimentary oxygenation variations**

441 Our observed pattern of RSEs in core CSH1 suggests that drastic changes in
442 sedimentary oxygenation occurred on orbital and millennial timescales over the last
443 glaciation in the OT. In general, four factors can regulate the redox condition in the
444 deep water column: (i) O₂ solubility, (ii) export productivity and subsequent
445 degradation of organic matter, (iii) vertical mixing, and (iv) lateral supply of oxygen
446 through intermediate and deeper water masses (Ivanochko and Pedersen, 2004;
447 Jaccard and Galbraith, 2012). These processes have been invoked in previous studies
448 to explain the deglacial Pacific-wide variations in oxygenation by either one or a
449 combination of these factors (Galbraith and Jaccard, 2015; Moffitt et al., 2015;

450 Praetorius et al., 2015). Our data also suggest drastic variations in sedimentary
451 oxygenation over the last 50 ka. However, the mechanisms responsible for
452 sedimentary oxygenation variations in the basin-wide OT and its connection with
453 ventilation of the open North Pacific remain unclear. In order to place our core results
454 in a wider regional context, we compare our proxy records of sedimentary
455 oxygenation (U_{excess} concentration and Mo/Mn ratio) and export productivity (CaCO_3)
456 (Figures 6a-6c) with abundance of *Pulleniatina obliquiloculata* (an indicator of
457 Kuroshio strength) and sea surface temperature (Shi et al., 2014), bulk sedimentary
458 nitrogen isotope (an indicator of denitrification) (Kao et al., 2008), benthic
459 foraminifera $\delta^{13}\text{C}$ (a proxy for ventilation) in cores PN-3 and PC23A (Rella et al.,
460 2012; Wahyudi and Minagawa, 1997), abundance of benthic foraminifera (an
461 indicator of hypoxia) in core E017 (Li et al., 2005) and ODP Site 1017 (Cannariato
462 and Kennett, 1999) (Figures 6d-6k).

463 **6.2.1. Effects of regional ocean temperature on deglacial deoxygenation**

464 Warming ocean temperatures lead to lower oxygen solubility. In the geological
465 past, solubility effects connected to temperature changes of the water column thought
466 to enhance or even trigger hypoxia (Praetorius et al., 2015). Shi et al. (2014) reported
467 an increase in SST of around 4°C (from $\sim 21^\circ\text{C}$ to $\sim 24.6^\circ\text{C}$) during the last
468 deglaciation in core CSH1 (Figure 6d). Based on thermal solubility effects, a
469 hypothetical warming of 1°C would reduce oxygen concentrations by about 3.5
470 $\mu\text{mol/kg}$ at water temperatures around 22°C (Brewer and Peltzer, 2016), therefore a \sim
471 4°C warming at core CSH1 (Shi et al., 2014) could drive a conservative estimate of a
472 drop of $<15 \mu\text{mol/kg}$ in oxygen concentration, assuming no large salinity changes.
473 However, given the semi-quantitative nature of our data about oxygenation changes,
474 which seemingly exceed an amplitude of $>15 \mu\text{mol/kg}$, we suggest that other factors,
475 e.g. local changes in export productivity, regional influences such as vertical mixing
476 due to changes of the Kuroshio Current, and far-field effects may have played
477 decisive roles in shaping the oxygenation history of the OT.

478 **6.2.2. Links between deglacial primary productivity and sedimentary** 479 **deoxygenation**

480 Previous studies have suggested the occurrence of high primary productivity in
481 the entire OT during the last deglacial period (Chang et al., 2009; Jian et al., 1996;
482 Kao et al., 2008; Li et al., 2017; Shao et al., 2016; Wahyudi and Minagawa, 1997).
483 Such an increase in export production was due to favorable conditions for
484 phytoplankton blooms, which were likely induced by warm temperatures and maxima
485 in nutrient availability, the latter being mainly sourced from increased discharge of
486 the Changjiang River, erosion of material from the ongoing flooding of the shallow
487 continental shelf in the ECS, and upwelling of Kuroshio Intermediate Water (Chang
488 et al., 2009; Li et al., 2017; Shao et al., 2016; Wahyudi and Minagawa, 1997). On the
489 basis of sedimentary reactive phosphorus concentration, Li et al. (2017) concluded
490 that export productivity increased during warm episodes but decreased during cold
491 spells on millennial timescales over the last 91 ka in the OT. Gradually increasing
492 concentrations of CaCO₃ in core CSH1 during the deglaciation (Figure 6a) and little
493 changes in foraminiferal fragmentation ratios (Wu et al., 2004), are indicative of high
494 export productivity in the northern OT. Accordingly, our data indicate that an increase
495 in export productivity during the last deglaciation, which was previously evidenced by
496 concentrations of reactive phosphorus (Li et al., 2017) and CaCO₃ (Chang et al., 2009)
497 from the middle OT, and thus was a pervasive, synchronous phenomenon in the entire
498 study region at the outermost extension of the ECS.

499 Similar events of high export productivity have been reported in the entire North
500 Pacific due to increased nutrient supply, high SST, reduced sea ice cover, etc.
501 (Crusius et al., 2004; Dean et al., 1997; Galbraith et al., 2007; Jaccard and Galbraith,
502 2012; Kohfeld and Chase, 2011). In most of these cases, increased export productivity
503 was thought to be responsible for oxygen depletion in mid-depth waters, due to
504 exceptionally high oxygen consumption. However, the productivity changes during
505 the deglacial interval, very specifically CaCO₃, are not fully consistent with the trends
506 of excess U and Mo/Mn ratio (Figures 6b and 6c). The sedimentary oxygenation thus
507 cannot be determined by export productivity alone.

508 **6.2.3 Effects of the Kuroshio dynamics on sedimentary oxygenation**

509 The Kuroshio Current, one of the main drivers of vertical mixing, has been

510 identified as the key factor in controlling modern deep ventilation in the OT (Kao et
511 al., 2006). However, the flow path of the Kuroshio in the OT during the glacial
512 interval remains a matter of debate. Planktic foraminiferal assemblages in sediment
513 cores from inside and outside the OT indicated that the Kuroshio migrated to the east
514 of the Ryukyu Islands during the LGM (Ujiié and Ujiié, 1999). Subsequently, Kao et
515 al. (2006) based on modeling results suggested that the Kuroshio still enters the OT,
516 but the volume transport was reduced by 43% compared to the present-day transport
517 and the outlet of Kuroshio switches from the Tokara Strait to the Kerama Gap at -80
518 and -135m lowered sea level. Combined with sea surface temperature (SST) records
519 and ocean model results, Lee et al. (2013) argued that there was little effect of
520 deglacial sea-level change on the path of the Kuroshio, which still exited the OT from
521 the Tokara Strait during the glacial period. Because the main stream of the Kuroshio
522 Current is at a water depth of ~150 m, the SST records are insufficient to decipher past
523 changes of the Kuroshio (Ujiié et al., 2016). On the other hand, low abundances of *P.*
524 *obliquiloculata* in core CSH1 in the northern OT (Figure 6e) indicate that the main
525 flow path of the Kuroshio migrated to the east of the Ryukyu Island (Shi et al., 2014).
526 Such a flow change would have been caused by the proposed block of the
527 Ryukyu-Taiwan land bridge by low sea level (Ujiié and Ujiié, 1999) and an overall
528 reduced Kuroshio intensity (Kao et al., 2006), effectively suppressing the effect of the
529 Kuroshio on deep ventilation in the OT. Our RSEs data show that oxygenated
530 sedimentary conditions were dominant in the northern OT throughout the last glacial
531 period (Figures 6b and 6c). The Kuroshio thus likely had a weak or even no effect on
532 the renewal of oxygen to the sedimentary environment during the last glacial period.
533 More recently, lower hydrothermal total Hg concentration during 20 ka - 9.6 ka,
534 associated with reduced intensity and/or variation in flow path of KC, relative to that
535 of Holocene recorded in core KX12 - 3 (1423 water depth) (Lim et al., 2017), further
536 validates our inference.

537 On the other hand, the gradually increased alkenone-derived SST and abundance
538 of *P.obliquiloculata* (Figures 6d and 6e) from 15 ka onwards indicates an intensified
539 Kuroshio Current. At present, mooring and float observations revealed that the KC

540 penetrates to 1200 m isobath in the East China Sea (Andres et al., 2015). However,
541 the effect of Kuroshio on sedimentary oxygenation was likely very limited during the
542 glacial period and only gradually increasing throughout the last glacial termination.
543 Therefore, while its effect on our observed deglacial variation in oxygenation may
544 provide a slowly changing background condition in vertical mixing effects on the
545 sedimentary oxygenation in the OT, it cannot account for the first order, rapid
546 oxygenation changes, including indications for millennial-scale variations, that we
547 observe between 18 ka and 9 ka.

548 Better oxygenated sedimentary conditions since 8.5 ka coincided with intensified
549 Kuroshio (Li et al., 2005; Shi et al., 2014), as indicated by rapidly increased SST and
550 *P. obliquiloculata* abundance in core CSH1 (Figures 6d and 6e) and *C.hyalinea*
551 abundance in core E017 (Figure 6i). Re-entrance of the Kuroshio into the OT (Shi et
552 al., 2014) with rising eustatic sea level likely enhanced the vertical mixing and
553 exchange between bottom and surface waters, ventilating the deep water in the OT.
554 Previous comparative studies based on epibenthic $\delta^{13}\text{C}$ values indicated
555 well-ventilated deep water feeding both inside the OT and outside off the Ryukyu
556 Islands during the Holocene (Kubota et al., 2015; Wahyudi and Minagawa, 1997). In
557 summary, enhanced sedimentary oxygenation regime observed in the OT during the
558 Holocene is mainly related to the intensified Kuroshio, while the effect of the
559 Kuroshio on OT oxygenation was limited before 15 ka.

560 **6.2.4. Effects of GNPIW on sedimentary oxygenation**

561 Relatively stronger oxygenated Glacial North Pacific Intermediate Water
562 (GNPIW), coined by (Matsumoto et al., 2002), has been widely documented in the
563 Bering Sea (Itaki et al., 2012; Kim et al., 2011; Rella et al., 2012), the Okhotsk Sea
564 (Itaki et al., 2008; Okazaki et al., 2014; Okazaki et al., 2006; Wu et al., 2014), off east
565 Japan (Shibahara et al., 2007), the eastern North Pacific (Cartapanis et al., 2011;
566 Ohkushi et al., 2013) and western subarctic Pacific (Keigwin, 1998; Matsumoto et al.,
567 2002). The intensified formation of GNPIW due to additional source region in the
568 Bering Sea was proposed by Ohkushi et al. (2003) and Horikawa et al. (2010). Under
569 such conditions, the invasion of well-ventilated GNPIW into the OT through the

570 Kerama Gap would have replenished the water column oxygen in the OT, although
571 the penetration depth of GNPIW remains under debate (Jaccard and Galbraith, 2013;
572 Max et al., 2014; Okazaki et al., 2010; Rae et al., 2014). Both a gradual decrease in
573 excess U concentration and an increase in Mo/Mn ratio during the last glacial period
574 (25 ka-50 ka) validate such inference, suggesting pronounced effects of intensified
575 NPIW formation in the OT.

576 During HS1, a stronger formation of GNPIW was supported by proxy studies
577 and numerical simulations. For example, on the basis of paired benthic-planktic (B-P)
578 ¹⁴C data, enhanced penetration of NPIW into a much deeper water depth during HS1
579 relative to the Holocene has been revealed in several studies (Max et al., 2014;
580 Okazaki et al., 2010; Sagawa and Ikehara, 2008), which was also simulated by several
581 models (Chikamoto et al., 2012; Gong et al., 2019; Okazaki et al., 2010). On the other
582 hand, increased intermediate water temperature in the subtropical Pacific recorded in
583 core GH08-2004 (1166 m water depth) (Kubota et al., 2015) and young deep water
584 observed in the northern South China Sea during HS1 (Wan and Jian, 2014) along
585 downstream region of NPIW are also related to intensified NPIW formation.
586 Furthermore, the pathway of GNPIW from numerical model simulations (Zheng et al.,
587 2016) was similar to modern observations (You, 2003). Thus, all these evidence imply
588 a persistent, cause and effect relation between GNPIW ventilation, the intermediate
589 and deep water oxygen concentration in the OT and sediment redox state during HS1.
590 In addition, our RSEs data also suggested a similarly enhanced ventilation in HS2
591 (Figures 6b and 6c) that is also attributed to intensified GNPIW formation.

592 Hypoxic conditions during the B/A have been also widely observed in the mid-
593 and high-latitude North Pacific (Jaccard and Galbraith, 2012; Praetorius et al., 2015).
594 Our data of excess U concentration and Mo/Mn ratio recorded in core CSH1 (Figures
595 6b and 6c), together with enhanced denitrification and *B.aculeata* abundance (Figures
596 6f and 6h), further reveal the expansion of oxygen-depletion at mid-depth waters
597 down to the subtropical NW Pacific during the late deglacial period. Based on high
598 relative abundances of radiolarian species, indicators of upper intermediate water
599 ventilation in core PC-23A, Itaki et al. (2012) suggested that a presence of

600 well-ventilated waters was limited to the upper intermediate layer (200 m–500 m) in
601 the Bering Sea during warm periods, such as the B/A and Preboreal. Higher B-P
602 foraminiferal ^{14}C ages, together with increased temperature and salinity at
603 intermediate waters recorded in core GH02-1030 (off East Japan) supported a
604 weakened formation of NPIW during the B/A (Sagawa and Ikehara, 2008). These
605 lines of evidence indicate that the boundary between GNPIW and North Pacific Deep
606 Water shoaled during the B/A, in comparison to HS1. Based on a comparison of two
607 benthic foraminiferal oxygen and carbon isotope records from off northern Japan and
608 the southern Ryukyu Island, Kubota et al. (2015) found a stronger influence of Pacific
609 Deep Water on intermediate-water temperature and ventilation at their southern than
610 the northern locations, though both sites are located at similar water depths (1166 m
611 and 1212 m for cores GH08-2004 and GH02-1030, respectively). Higher excess U
612 concentration and low Mo/Mn ratio in our core CSH1 during the B/A and Preboreal
613 suggest reduced sedimentary oxygenation, consistent with reduced ventilation of
614 GNPIW, contributing to the subsurface water deoxygenation in the OT.

615 During the YD, both Mo/Mn ratio and excess U show a slightly decreased
616 oxygen condition in the northern OT. By contrast, benthic foraminiferal $\delta^{18}\text{O}$ and $\delta^{13}\text{C}$
617 values in a sediment core collected from the Oyashio region suggested a strengthened
618 formation and ventilation of GNPIW during the YD (Ohkushi et al., 2016). This
619 pattern possibly indicates a time-dependent, varying contribution of distal GNPIW to
620 the deglacial OT oxygenation history, and we presume a more pronounced
621 contribution of organic matter degradation due to high export productivity during this
622 period, as suggested by increasing CaCO_3 content.

623 **6.3. Subtropical North Pacific ventilation links to North Atlantic Climate**

624 One of the characteristic climate features in the Northern Hemisphere, in
625 particular the North Atlantic is millennial-scale oscillation during glacial and deglacial
626 periods. These abrupt climatic events have been widely thought to be closely related
627 to varying strength of Atlantic Meridional Overturning Circulation (AMOC)
628 (Lynch-Stieglitz, 2017). One of dynamic proxies of ocean circulation, $^{231}\text{Pa}/^{230}\text{Th}$
629 reveals that severe weakening of AMOC only existed during Heinrich stadials due to

630 increased freshwater discharges into the North Atlantic (Böhm et al., 2015; McManus
631 et al., 2004). On the other hand, several mechanisms, such as sudden termination of
632 freshwater input (Liu et al., 2009), atmospheric CO₂ concentration (Zhang et al.,
633 2017), enhanced advection of salt (Barker et al., 2010) and changes in background
634 climate (Knorr and Lohmann, 2007) were proposed to explain the reinvigoration of
635 AMOC during the B/A.

636 Our RSEs data in the Northern OT and endobenthic $\delta^{13}\text{C}$ in the Bering Sea
637 (Figures 7a-7c) both show a substantial millennial variability in intermediate water
638 ventilation in the subtropical North Pacific. Notably, enhanced ventilation during HS1
639 and HS2 and oxygen-poor condition during the B/A respectively correspond to the
640 collapse and resumption of AMOC (Figure 7d). Such out-of-phase millennial-scale
641 pattern is consistent with the results of various modeling simulations (Chikamoto et
642 al., 2012; Menviel et al., 2014; Okazaki et al., 2010; Saenko et al., 2004), although
643 these models had different boundary conditions and causes for the observed effects in
644 GNPIW formation, and ventilation ages derived from B-P ^{14}C (Freeman et al., 2015;
645 Max et al., 2014; Okazaki et al., 2012). These lines of evidence confirm a persistent
646 link between the ventilation of North Pacific and the North Atlantic climate
647 (Lohmann et al., 2019). Such links have also been corroborated by proxy data and
648 modeling experiment between AMOC and East Asian monsoon during the 8.2 ka
649 event (Liu et al., 2013), the Holocene (Wang et al., 2005) and 34 ka–60 ka (Sun et al.,
650 2012). The mechanism linking East Asia with North Atlantic has been attributed to an
651 atmospheric teleconnection, such as the position and strength of Westerly Jet and
652 Mongolia-Siberian High (Porter and Zhisheng, 1995). However, the mechanism
653 behind such out-of-phase pattern between the ventilation in the subtropical North
654 Pacific and the North Atlantic deep water formation remains unclear.

655 Increased NPIW formation during HS1 may have been caused by enhanced
656 salinity-driven vertical mixing through higher meridional water mass transport from
657 the subtropical Pacific. Previous studies have proposed that intermediate water
658 formation in the North Pacific hinged on a basin-wide increase in sea surface salinity
659 driven by changes in strength of the summer EAM and the moisture transport from

660 the Atlantic to the Pacific (Emile-Geay et al., 2003). Several modeling studies found
661 that freshwater forcing in the North Atlantic could cause a widespread surface
662 salinification in the subtropical Pacific Ocean (Menviel et al., 2014; Okazaki et al.,
663 2010; Saenko et al., 2004). This idea has been tested by proxy data (Rodríguez-Sanz
664 et al., 2013; Sagawa and Ikehara, 2008), which indicated a weakened summer EAM
665 and reduced transport of moisture from Atlantic to Pacific through Panama Isthmus
666 owing to the southward displacement of Intertropical Convergence Zone caused by a
667 weakening of AMOC. Along with this process, as predicted through a general
668 circulation modeling, a strengthened Pacific Meridional Overturning Circulation
669 would have transported more warm and salty subtropical water into the high-latitude
670 North Pacific (Okazaki et al., 2010). In accordance with comprehensive Mg/Ca
671 ratio-based salinity reconstructions, however, Riethdorf et al. (2013) found no clear
672 evidence for such higher salinity patterns in the subarctic northwest Pacific during
673 HS1.

674 On the other hand, a weakened AMOC would deepen the wintertime Aleutian
675 Low based on modern observation (Okumura et al., 2009), which is closely related to
676 the sea ice formation in the marginal seas of the subarctic Pacific (Cavalieri and
677 Parkinson, 1987). Once stronger Aleutian Low, intense brine rejection due to sea ice
678 expansion, would have enhanced the NPIW formation. Recently modeling-derived
679 evidence confirmed that enhanced sea ice coverage occurred in the southern Okhotsk
680 Sea and off East Kamchatka Peninsula during HS1 (Gong et al., 2019). In addition,
681 stronger advection of low-salinity water via the Alaskan Stream to the subarctic NW
682 Pacific was probably enhanced during HS1, related to a shift of the Aleutian Low
683 pressure system over the North Pacific, which could also increase sea ice formation,
684 brine rejection and thereafter intermediate water ventilation (Riethdorf et al., 2013).

685 During the late deglaciation, ameliorating global climate conditions, such as
686 warming Northern Hemisphere, and a strengthened Asian summer monsoon, are a
687 result of changes in insolation forcing, greenhouse gases concentrations, and variable
688 strengths of the AMOC (Clark et al., 2012; Liu et al., 2009). During the B/A, a
689 decrease in sea ice extent and duration was indicated by combined reconstructions of

690 SST and mixed layer temperatures from the subarctic Pacific (Riethdorf et al., 2013).
691 At that time, the rising eustatic sea level (Spratt and Lisiecki, 2016) would have
692 supported the intrusion of Alaska Stream into the Bering Sea by deepening and
693 opening glacial closed straits of the Aleutian Islands chain, while reducing the
694 advection of the Alaska Stream to the subarctic Pacific gyre (Riethdorf et al., 2013).
695 In this scenario, saltier and more stratified surface water conditions would have
696 inhibited brine rejection and subsequent formation and ventilation of NPIW (Lam et
697 al., 2013), leading to a reorganization of the Pacific water mass, closely coupled to the
698 collapse and resumption modes of the AMOC during these two intervals.

699 **6.4 Increased storage of CO₂ at mid-depth water in the North Pacific at the B/A**

700 One of the striking features of RSEs data is higher Mo/Mn ratios and excess U
701 concentrations across the B/A, supporting an expansion of Oxygen Minimum Zone in
702 the North Pacific (Galbraith and Jaccard, 2015; Jaccard and Galbraith, 2012; Moffitt
703 et al., 2015) and coinciding with the termination of atmospheric CO₂ concentration
704 rise (Marcott et al., 2014) (Figure 7e). As described above, it can be related to the
705 upwelling of nutrient- and CO₂-rich Pacific Deep Water due to resumption of AMOC
706 and enhanced export production. Notably, boron isotope data measured on
707 surface-dwelling foraminifera in core MD01-2416 situated in the western subarctic
708 North Pacific did reveal a decrease in near-surface pH and an increase in pCO₂ at the
709 onset of B/A (Gray et al., 2018), indicating that the subarctic North Pacific is a source
710 of relatively high atmospheric CO₂ concentration at that time. Here we cannot
711 conclude that the same processes could have occurred in the subtropical North Pacific
712 due to the lack of well-known drivers to draw out of the old carbon in the deep sea
713 into the atmosphere. In combination with published records from the North Pacific
714 (Addison et al., 2012; Cartapanis et al., 2011; Crusius et al., 2004; Galbraith et al.,
715 2007; Lembke-Jene et al., 2017; Shibahara et al., 2007), an expansion of
716 oxygen-depletion zone during the B/A suggest an increase in respired carbon storage
717 at mid-depth waters of the North Pacific, which likely stalls the rise of atmospheric
718 CO₂. Our results support the findings by Galbraith et al. (2007). Given the sizeable
719 volume of the North Pacific, potentially, once the respired carbon could be emitted to

720 the atmosphere in stages, which would bring the planet out of the last ice age (Jaccard
721 and Galbraith, 2018).

722 **7. Conclusions**

723 Our geochemical results of sediment core CSH1 revealed substantial changes in
724 intermediate water redox conditions in the northern Okinawa Trough over the last 50
725 ka on orbital and millennial timescales. Enhanced sedimentary oxygenation mainly
726 occurred during cold intervals, such as the last glacial period, Heinrich stadials 1 and
727 2, and during the middle and late Holocene, while diminished sedimentary
728 oxygenation prevailed during the Bölling-Alleröd and Preboreal. The sedimentary
729 oxygenation variability presented here provides key evidence for the substantial
730 impact of ventilation of NPIW on the sedimentary oxygenation in the subtropical
731 North Pacific and shows out-of-phase pattern with North Atlantic Climate during the
732 last deglaciation. The linkage is attributable to the disruption of NPIW formation
733 caused by climate changes in the North Atlantic, which is transferred to the North
734 Pacific via atmospheric and oceanic teleconnections. We also suggest an expansion of
735 oxygen-depleted zone and accumulation of respired carbon at the mid-depth waters
736 from previously reported subarctic locations into the western subtropical the North
737 Pacific during the B/A, coinciding with the termination of atmospheric CO₂ rise. A
738 step-wise injection of such respired carbon into the atmosphere would be helpful to
739 maintain high atmospheric CO₂ levels during the deglaciation and bring the planet out
740 of the last ice age.

741

742 **Data availability.** All raw data are available to all interested researchers upon request.

743

744 **Author Contributions.** J.J.Z. and X.F.S. conceived the study. A.M.Z. performed
745 geochemical analyses of bulk sediments. J.J.Z., X.F.S. K.S. and X.G. led the write up
746 of the manuscript. All other authors provided comments on the manuscript and
747 contributed to the final version of the manuscript.

748

749 **Competing interests:** The authors declare no competing interests.

750

751 **Acknowledgements**

752 Financial support was provided by the National Program on Global Change and
753 Air-Sea Interaction (GASI-GEOGE-04), by the National Natural Science Foundation
754 of China (Grant Nos.: 41476056, 41876065, 41420104005, 41206059, and U1606401)
755 and by the Basic Scientific Fund for National Public Research Institutes of China
756 (No.2016Q09) and International Cooperative Projects in Polar Study (201613) and
757 Taishan Scholars Program of Shandong. This study is a contribution to the bilateral
758 Sino-German collaboration project (funding through BMBF grant 03F0704A –
759 SIGEPAX). XG, LLJ, GL, RT thank the bilateral Sino-German collaboration
760 NOPAWAC project (BMBF grant No. 03F0785A).LLJ and RT acknowledge financial
761 support through the national Helmholtz REKLIM Initiative. We would like to thank
762 the anonymous reviewers, who helped to improve the quality of this manuscript. The
763 data used in this study are available from the authors upon request
764 (zoujianjun@fio.org.cn).

765

766 **References**

- 767 Addison, J. A., Finney, B. P., Dean, W. E., Davies, M. H., Mix, A. C., Stoner, J. S., and Jaeger, J.
768 M.: Productivity and sedimentary $\delta^{15}\text{N}$ variability for the last 17,000 years along the northern Gulf
769 of Alaska continental slope, *Paleoceanography*, 27, PA1206, doi:1210.1029/2011PA002161, 2012.
- 770 Algeo, T. J.: Can marine anoxic events draw down the trace element inventory of seawater?,
771 *Geology*, 32, 1057-1060, 2004.
- 772 Algeo, T. J. and Lyons, T. W.: Mo-total organic carbon covariation in modern anoxic marine
773 environments: Implications for analysis of paleoredox and paleohydrographic conditions,
774 *Paleoceanography*, 21, PA1016, doi: 1010.1029/2004pa001112, 2006.
- 775 Algeo, T. J. and Tribovillard, N.: Environmental analysis of paleoceanographic systems based on
776 molybdenum–uranium covariation, *Chemical Geology*, 268, 211-225, 2009.
- 777 Andres, M., Jan, S., Sanford, T. B., Mensah, V., Centurioni, L. R., and Book, J. W.: Mean structure
778 and variability of the Kuroshio from northeastern Taiwan to southwestern Japan, *Oceanography*,
779 26, 84–95, 2015.
- 780 Böhm, E., Lippold, J., Gutjahr, M., Frank, M., Blaser, P., Antz, B., Fohlmeister, J., Frank, N.,
781 Andersen, M. B., and Deininger, M.: Strong and deep Atlantic meridional overturning circulation
782 during the last glacial cycle, *Nature*, 517, 73-76, 2015.
- 783 Barker, S., Knorr, G., Vautravers, M. J., Diz, P., and Skinner, L. C.: Extreme deepening of the
784 Atlantic overturning circulation during deglaciation, *Nature Geoscience*, 3, 567-571, 2010.
- 785 Beny, F., Toucanne, S., Skonieczny, C., Bayon, G., and Ziegler, M.: Geochemical provenance of

786 sediments from the northern East China Sea document a gradual migration of the Asian Monsoon
787 belt over the past 400,000 years, *Quaternary Science Reviews*, 190, 161-175, 2018.

788 Bianchi, D., Dunne, J. P., Sarmiento, J. L., and Galbraith, E. D.: Data-based estimates of suboxia,
789 denitrification, and N₂O production in the ocean and their sensitivities to dissolved O₂, *Global*
790 *Biogeochemical Cycles*, 26, doi:10.1029/2011gb004209, 2012.

791 Brewer, P. G. and Peltzer, E. T.: Ocean chemistry, ocean warming, and emerging hypoxia:
792 Commentary, *Journal of Geophysical Research: Oceans*, 121, 3659-3667, 2016.

793 Burdige, D. J.: The biogeochemistry of manganese and iron reduction in marine sediments,
794 *Earth-Science Reviews*, 35, 249-284, 1993.

795 Cannariato, K. G. and Kennett, J. P.: Climatically related millennial-scale fluctuations in strength
796 of California margin oxygen-minimum zone during the past 60 k.y, *Geology*, 27, 975-978, 1999.

797 Cartapanis, O., Tachikawa, K., and Bard, E.: Northeastern Pacific oxygen minimum zone
798 variability over the past 70 kyr: Impact of biological production and oceanic ventilation,
799 *Paleoceanography*, 26, PA4208, doi: 4210.1029/2011PA002126, 2011.

800 Cavalieri, D. J. and Parkinson, C. L.: On the relationship between atmospheric circulation and the
801 fluctuations in the sea ice extents of the bering and okhotsk seas, *Journal of Geophysical*
802 *Research-Oceans*, 92, 7141-7162, 1987.

803 Chang, A. S., Pedersen, T. F., and Hendy, I. L.: Effects of productivity, glaciation, and ventilation
804 on late Quaternary sedimentary redox and trace element accumulation on the Vancouver Island
805 margin, western Canada, *Paleoceanography*, 29, doi: 10.1002/2013PA002581, 2014.

806 Chang, Y.-P., Chen, M.-T., Yokoyama, Y., Matsuzaki, H., Thompson, W. G., Kao, S.-J., and
807 Kawahata, H.: Monsoon hydrography and productivity changes in the East China Sea during the
808 past 100,000 years: Okinawa Trough evidence (MD012404), *Paleoceanography*, 24, PA3208, doi:
809 3210.1029/2007PA001577, 2009.

810 Chen, J., Zhang, D., Zhang, W., and Li, T.: The paleoclimatic change since the last galciation in
811 the north of Okinawa Trough based on the spore-pollen records, *Acta Oceanologica Sinica*, 28,
812 85-91, 2006 (in Chinese with English Abstract).

813 Cheng, H., Edwards, R. L., Sinha, A., Spötl, C., Yi, L., Chen, S., Kelly, M., Kathayat, G., Wang,
814 X., Li, X., Kong, X., Wang, Y., Ning, Y., and Zhang, H.: The Asian monsoon over the past 640,000
815 years and ice age terminations, *Nature*, 534, 640-646, 2016.

816 Cheng, H., Edwards, R. L., Southon, J., Matsumoto, K., Feinberg, J. M., Sinha, A., Zhou, W., Li,
817 H., Li, X., Xu, Y., Chen, S., Tan, M., Wang, Q., Wang, Y., and Ning, Y.: Atmospheric 14C/12C
818 changes during the last glacial period from Hulu Cave, *Science*, 362, 1293-1297, 2018.

819 Chikamoto, M. O., Menviel, L., Abe-Ouchi, A., Ohgaito, R., Timmermann, A., Okazaki, Y.,
820 Harada, N., Oka, A., and Mouchet, A.: Variability in North Pacific intermediate and deep water
821 ventilation during Heinrich events in two coupled climate models, *Deep Sea Research Part II:*
822 *Topical Studies in Oceanography*, 61-64, 114-126, 2012.

823 Clark, P. U., Shakun, J. D., Baker, P. A., Bartlein, P. J., Brewer, S., Brook, E., Carlson, A. E.,
824 Cheng, H., Kaufman, D. S., Liu, Z., Marchitto, T. M., Mix, A. C., Morrill, C., Otto-Bliesner, B. L.,
825 Pahnke, K., Russell, J. M., Whitlock, C., Adkins, J. F., Blois, J. L., Clark, J., Colman, S. M., Curry,
826 W. B., Flower, B. P., He, F., Johnson, T. C., Lynch-Stieglitz, J., Markgraf, V., McManus, J.,
827 Mitrovica, J. X., Moreno, P. I., and Williams, J. W.: Global climate evolution during the last
828 deglaciation, *Proceedings of the National Academy of Sciences of the United States of America*,
829 109, E1134-E1142, 2012.

830 Clemens, S. C., Holbourn, A., Kubota, Y., Lee, K. E., Liu, Z., Chen, G., Nelson, A., and
831 Fox-Kemper, B.: Precession-band variance missing from East Asian monsoon runoff, *Nature*
832 *Communications*, 9, 3364, doi: 3310.1038/s41467-41018-05814-41460, 2018.

833 Crusius, J., Calvert, S., Pedersen, T., and Sage, D.: Rhenium and molybdenum enrichments in
834 sediments as indicators of oxic, suboxic and sulfidic conditions of deposition, *Earth and Planetary*
835 *Science Letters*, 145, 65-78, 1996.

836 Crusius, J., Pedersen, T. F., Kienast, S., Keigwin, L., and Labeyrie, L.: Influence of northwest
837 Pacific productivity on North Pacific Intermediate Water oxygen concentrations during the
838 Boiling-Allerod interval (14.7-12.9 ka), *Geology*, 32, 633-636, 2004.

839 Dahl, T. W., Anbar, A. D., Gordon, G. W., Rosing, M. T., Frei, R., and Canfield, D. E.: The
840 behavior of molybdenum and its isotopes across the chemocline and in the sediments of sulfidic
841 Lake Cadagno, Switzerland, *Geochimica et Cosmochimica Acta*, 74, 144-163, 2010.

842 Dean, W. E., Gardner, J. V., and Piper, D. Z.: Inorganic geochemical indicators of
843 glacial-interglacial changes in productivity and anoxia on the California continental margin,
844 *Geochimica et Cosmochimica Acta*, 61, 4507-4518, 1997.

845 Delcroix, T. and Murtugudde, R.: Sea surface salinity changes in the East China Sea during
846 1997–2001: Influence of the Yangtze River, *Journal of Geophysical Research: Oceans*, 107, 8008,
847 doi:8010.1029/2001JC000893, 2002.

848 Dou, Y., Yang, S., Li, C., Shi, X., Liu, J., and Bi, L.: Deepwater redox changes in the southern
849 Okinawa Trough since the last glacial maximum, *Progress in Oceanography*, 135, 77-90, 2015.

850 Emile-Geay, J., Cane, M. A., Naik, N., Seager, R., Clement, A. C., and van Geen, A.: Warren
851 revisited: Atmospheric freshwater fluxes and “Why is no deep water formed in the North Pacific”,
852 *Journal of Geophysical Research: Oceans*, 108, doi:10.1029/2001JC001058, 2003.

853 Freeman, E., Skinner, L. C., Tisserand, A., Dokken, T., Timmermann, A., Menviel, L., and
854 Friedrich, T.: An Atlantic–Pacific ventilation seesaw across the last deglaciation, *Earth and*
855 *Planetary Science Letters*, 424, 237-244, 2015.

856 Galbraith, E. D. and Jaccard, S. L.: Deglacial weakening of the oceanic soft tissue pump: global
857 constraints from sedimentary nitrogen isotopes and oxygenation proxies, *Quaternary Science*
858 *Reviews*, 109, 38-48, 2015.

859 Galbraith, E. D., Jaccard, S. L., Pedersen, T. F., Sigman, D. M., Haug, G. H., Cook, M., Southon, J.
860 R., and Francois, R.: Carbon dioxide release from the North Pacific abyss during the last
861 deglaciation, *Nature*, 449, 890-893, 2007.

862 Galbraith, E. D., Kienast, M., Pedersen, T. F., and Calvert, S. E.: Glacial-interglacial modulation
863 of the marine nitrogen cycle by high-latitude O₂ supply to the global thermocline,
864 *Paleoceanography*, 19, PA4007, doi:4010.1029/2003PA001000, 2004.

865 Ge, S., Shi, X., Wu, Y., Lee, T., Xiong, Y., and Saito, Y.: Rock magnetic property of gravity core
866 CSH1 from the northern Okinawa Trough and the effect of early diagenesis, *Acta Oceanologica*
867 *Sinica*, 26, 54-65, 2007.

868 Gong, X., Lembke-Jene, L., Lohmann, G., Knorr, G., Tiedemann, R., Zou, J. J., and Shi, X. F.:
869 Enhanced North Pacific deep-ocean stratification by stronger intermediate water formation during
870 Heinrich Stadial 1, *Nature Communications*, 10, 656, doi:610.1038/s41467-41019-08606-41462,
871 2019.

872 Gray, W. R., Rae, J. W. B., Wills, R. C. J., Shevenell, A. E., Taylor, B., Burke, A., Foster, G. L.,
873 and Lear, C. H.: Deglacial upwelling, productivity and CO₂ outgassing in the North Pacific Ocean,

874 Nature Geoscience, 11, 340-344, 2018.

875 Helz, G. R., Miller, C. V., Charnock, J. M., Mosselmans, J. F. W., Patrick, R. A. D., Garner, C. D.,
876 and Vaughan, D. J.: Mechanism of molybdenum removal from the sea and its concentration in
877 black shales: EXAFS evidence, *Geochimica et Cosmochimica Acta*, 60, 3631-3642, 1996.

878 Hofmann, A. F., Peltzer, E. T., Walz, P. M., and Brewer, P. G.: Hypoxia by degrees: Establishing
879 definitions for a changing ocean, *Deep Sea Research Part I: Oceanographic Research Papers*, 58,
880 1212-1226, 2011.

881 Hoogakker, B. A. A., Elderfield, H., Schmiedl, G., McCave, I. N., and Rickaby, R. E. M.:
882 Glacial–interglacial changes in bottom-water oxygen content on the Portuguese margin, *Nature*
883 *Geoscience*, 8, 40-43, 2015.

884 Horikawa, K., Asahara, Y., Yamamoto, K., and Okazaki, Y.: Intermediate water formation in the
885 Bering Sea during glacial periods: Evidence from neodymium isotope ratios, *Geology*, 38,
886 435-438, 2010.

887 Ichikawa, H. and Beardsley, R. C.: The Current System in the Yellow and East China Seas, *Journal*
888 *of Oceanography*, 58, 77-92, 2002.

889 Itaki, T., Khim, B. K., and Ikehara, K.: Last glacial-Holocene water structure in the southwestern
890 Okhotsk Sea inferred from radiolarian assemblages, *Marine Micropaleontology*, 67, 191-215,
891 2008.

892 Itaki, T., Kim, S., Rella, S. F., Uchida, M., Tada, R., and Khim, B. K.: Millennial-scale variations
893 of late Pleistocene radiolarian assemblages in the Bering Sea related to environments in shallow
894 and deep waters, *Deep-Sea Research Part II-Topical Studies in Oceanography*, 61-64, 127-144,
895 2012.

896 Ivanochko, T. S. and Pedersen, T. F.: Determining the influences of Late Quaternary ventilation
897 and productivity variations on Santa Barbara Basin sedimentary oxygenation: a multi-proxy
898 approach, *Quaternary Science Reviews*, 23, 467-480, 2004.

899 Jaccard, S. L. and Galbraith, E. D.: Direct ventilation of the North Pacific did not reach the deep
900 ocean during the last deglaciation, *Geophysical Research Letters*, 40, 199-203, 2013.

901 Jaccard, S. L. and Galbraith, E. D.: Large climate-driven changes of oceanic oxygen
902 concentrations during the last deglaciation, *Nature Geoscience*, 5, 151-156, 2012.

903 Jaccard, S. L. and Galbraith, E. D.: Push from the Pacific, *Nature Geoscience*, 11, 299-300, 2018.

904 Jaccard, S. L., Galbraith, E. D., Martínez-García, A., and Anderson, R. F.: Covariation of deep
905 Southern Ocean oxygenation and atmospheric CO₂ through the last ice age, *Nature*, 530, 207-210,
906 2016.

907 Jaccard, S. L., Galbraith, E. D., Sigman, D. M., Haug, G. H., Francois, R., Pedersen, T. F., Dulski,
908 P., and Thierstein, H. R.: Subarctic Pacific evidence for a glacial deepening of the oceanic respired
909 carbon pool, *Earth and Planetary Science Letters*, 277, 156-165, 2009.

910 Jian, Z. M., Chen, R. H., and Li, B. H.: Deep-sea benthic foraminiferal record of the
911 paleoceanography in the southern Okinawa trough over the last 20000 years, *Science in China*
912 *Series D-Earth Sciences*, 39, 551-560, 1996.

913 Kao, S. J., Horng, C. S., Hsu, S. C., Wei, K. Y., Chen, J., and Lin, Y. S.: Enhanced deepwater
914 circulation and shift of sedimentary organic matter oxidation pathway in the Okinawa Trough
915 since the Holocene, *Geophysical Research Letters*, 32, L15609, doi:15610.11029/12005GL023139,
916 2005.

917 Kao, S. J., Liu, K. K., Hsu, S. C., Chang, Y. P., and Dai, M. H.: North Pacific-wide spreading of

918 isotopically heavy nitrogen during the last deglaciation: Evidence from the western Pacific,
919 *Biogeosciences*, 5, 1641-1650, 2008.

920 Kao, S. J., Wu, C.-R., Hsin, Y.-C., and Dai, M.: Effects of sea level change on the upstream
921 Kuroshio Current through the Okinawa Trough, *Geophysical Research Letters*, 33, L16604,
922 doi:10.1029/2006gl026822, 2006.

923 Keigwin, L. D.: Glacial-age hydrography of the far northwest Pacific Ocean, *Paleoceanography*,
924 13, 323-339, 1998.

925 Kim, S., Khim, B. K., Uchida, M., Itaki, T., and Tada, R.: Millennial-scale paleoceanographic
926 events and implication for the intermediate-water ventilation in the northern slope area of the
927 Bering Sea during the last 71 kyrs, *Global and Planetary Change*, 79, 89-98, 2011.

928 Klinkhammer, G. P. and Palmer, M. R.: Uranium in the oceans: Where it goes and why,
929 *Geochimica et Cosmochimica Acta*, 55, 1799-1806, 1991.

930 Knorr, G. and Lohmann, G.: Rapid transitions in the Atlantic thermohaline circulation triggered by
931 global warming and meltwater during the last deglaciation, *Geochemistry, Geophysics,*
932 *Geosystems*, 8, DOI: 10.1029/2007gc001604, 2007.

933 Kohfeld, K. E. and Chase, Z.: Controls on deglacial changes in biogenic fluxes in the North
934 Pacific Ocean, *Quaternary Science Reviews*, 30, 3350-3363, 2011.

935 Kubota, Y., Kimoto, K., Itaki, T., Yokoyama, Y., Miyairi, Y., and Matsuzaki, H.: Bottom water
936 variability in the subtropical northwestern Pacific from 26 kyr BP to present based on Mg/Ca and
937 stable carbon and oxygen isotopes of benthic foraminifera, *Climate of the Past*, 11, 803-824, 2015.

938 Kubota, Y., Kimoto, K., Tada, R., Oda, H., Yokoyama, Y., and Matsuzaki, H.: Variations of East
939 Asian summer monsoon since the last deglaciation based on Mg/Ca and oxygen isotope of
940 planktic foraminifera in the northern East China Sea, *Paleoceanography*, 25, PA4205,
941 doi:10.1029/2009pa001891, 2010.

942 Lam, P. J., Robinson, L. F., Blusztajn, J., Li, C., Cook, M. S., McManus, J. F., and Keigwin, L. D.:
943 Transient stratification as the cause of the North Pacific productivity spike during deglaciation,
944 *Nature Geosci*, 6, 622-626, 2013.

945 Lee, K. E., Lee, H. J., Park, J.-H., Chang, Y.-P., Ikehara, K., Itaki, T., and Kwon, H. K.: Stability
946 of the Kuroshio path with respect to glacial sea level lowering, *Geophysical Research Letters*, 40,
947 392-396, doi:10.1002/grl.50102, 2013.

948 Lembke-Jene, L., Tiedemann, R., Nürnberg, D., Kokfelt, U., Kozdon, R., Max, L., Röhl, U., and
949 Gorbarenko, S. A.: Deglacial variability in Okhotsk Sea Intermediate Water ventilation and
950 biogeochemistry: Implications for North Pacific nutrient supply and productivity, *Quaternary*
951 *Science Reviews*, 160, 116-137, 2017.

952 Li, D., Zheng, L.-W., Jaccard, S. L., Fang, T.-H., Paytan, A., Zheng, X., Chang, Y.-P., and Kao,
953 S.-J.: Millennial-scale ocean dynamics controlled export productivity in the subtropical North
954 Pacific, *Geology*, 45, 651-654, 2017.

955 Li, T., Xu, Z., Lim, D., Chang, F., Wan, S., Jung, H., and Choi, J.: Sr-Nd isotopic constraints on
956 detrital sediment provenance and paleoenvironmental change in the northern Okinawa Trough
957 during the late Quaternary, *Palaeogeography, Palaeoclimatology, Palaeoecology*, 430, 74-84, 2015.

958 Li, T. G., Xiang, R., Sun, R. T., and Cao, Q. Y.: Benthic foraminifera and bottom water evolution
959 in the middle-southern Okinawa Trough during the last 18 ka, *Science in China Series D-Earth*
960 *Sciences*, 48, 805-814, 2005.

961 Li, Y. H. and Schoonmaker, J. E.: Chemical Composition and Mineralogy of Marine Sediments. In:

962 Treatise on Geochemistry (Second Edition), Turekian, K. K. (Ed.), Elsevier, Oxford, 2014.

963 Lim, D., Kim, J., Xu, Z., Jeong, K., and Jung, H.: New evidence for Kuroshio inflow and
964 deepwater circulation in the Okinawa Trough, East China Sea: Sedimentary mercury variations
965 over the last 20 kyr, *Paleoceanography*, 32, 571-579, 2017.

966 Liu, Y. H., Henderson, G. M., Hu, C. Y., Mason, A. J., Charnley, N., Johnson, K. R., and Xie, S. C.:
967 Links between the East Asian monsoon and North Atlantic climate during the 8,200 year event,
968 *Nature Geosci*, 6, 117-120, 2013.

969 Liu, Z., Otto-Bliesner, B. L., He, F., Brady, E. C., Tomas, R., Clark, P. U., Carlson, A. E.,
970 Lynch-Stieglitz, J., Curry, W., Brook, E., Erickson, D., Jacob, R., Kutzbach, J., and Cheng, J.:
971 Transient Simulation of Last Deglaciation with a New Mechanism for Bølling-Allerød Warming,
972 *Science*, 325, 310-314, 2009.

973 Lohmann, G., Lembke-Jene, L., Tiedemann, R., Gong, X., Scholz, P., Zou, J., and Shi, X.:
974 Challenges in the Paleoclimatic Evolution of the Arctic and Subarctic Pacific since the Last
975 Glacial Period—The Sino–German Pacific–Arctic Experiment (SiGePAX), *Challenges*, 10, 13,
976 doi:10.3390/challe10010013, 2019.

977 Lynch-Stieglitz, J.: The Atlantic Meridional Overturning Circulation and Abrupt Climate Change,
978 *Annual Review of Marine Science*, 9, 83-104, 2017.

979 Lyons, T. W., Anbar, A. D., Severmann, S., Scott, C., and Gill, B. C.: Tracking Euxinia in the
980 Ancient Ocean: A Multiproxy Perspective and Proterozoic Case Study, *Annual Review of Earth
981 and Planetary Sciences*, 37, 507-534, 2009.

982 Machida, H.: The stratigraphy, chronology and distribution of distal marker-tephras in and around
983 Japan, *Global and Planetary Change*, 21, 71-94, 1999.

984 Maithani, P. B. and Srinivasan, S.: Felsic Volcanic Rocks, a Potential Source of Uranium - An
985 Indian Overview, *Energy Procedia*, 7, 163-168, 2011.

986 Marcott, S. A., Bauska, T. K., Buizert, C., Steig, E. J., Rosen, J. L., Cuffey, K. M., Fudge, T. J.,
987 Severinghaus, J. P., Ahn, J., Kalk, M. L., McConnell, J. R., Sowers, T., Taylor, K. C., White, J. W.
988 C., and Brook, E. J.: Centennial-scale changes in the global carbon cycle during the last
989 deglaciation, *Nature*, 514, 616-619, 2014.

990 Matsumoto, K., Oba, T., Lynch-Stieglitz, J., and Yamamoto, H.: Interior hydrography and
991 circulation of the glacial Pacific Ocean, *Quaternary Science Reviews*, 21, 1693-1704, 2002.

992 Max, L., Lembke-Jene, L., Riethdorf, J. R., Tiedemann, R., Nurnberg, D., Kuhn, H., and
993 Mackensen, A.: Pulses of enhanced North Pacific Intermediate Water ventilation from the Okhotsk
994 Sea and Bering Sea during the last deglaciation, *Climate of the Past*, 10, 591-605, 2014.

995 Max, L., Rippert, N., Lembke-Jene, L., Mackensen, A., Nürnberg, D., and Tiedemann, R.:
996 Evidence for enhanced convection of North Pacific Intermediate Water to the low-latitude Pacific
997 under glacial conditions, *Paleoceanography*, 32, 41-55, 2017.

998 McManus, J., Berelson, W. M., Klinkhammer, G. P., Hammond, D. E., and Holm, C.: Authigenic
999 uranium: Relationship to oxygen penetration depth and organic carbon rain, *Geochimica et
1000 Cosmochimica Acta*, 69, 95-108, 2005.

1001 McManus, J. F., Francois, R., Gherardi, J. M., Keigwin, L. D., and Brown-Leger, S.: Collapse and
1002 rapid resumption of Atlantic meridional circulation linked to deglacial climate changes, *Nature*,
1003 428, 834-837, 2004.

1004 Menviel, L., England, M. H., Meissner, K. J., Mouchet, A., and Yu, J.: Atlantic-Pacific seesaw and
1005 its role in outgassing CO₂ during Heinrich events, *Paleoceanography*, 29, 58-70, 2014.

1006 Moffitt, S. E., Moffitt, R. A., Sauthoff, W., Davis, C. V., Hewett, K., and Hill, T. M.:
1007 Paleooceanographic Insights on Recent Oxygen Minimum Zone Expansion: Lessons for Modern
1008 Oceanography, PLOS ONE, 10, e0115246, doi, 0115210.0111371/journal.pone.0115246, 2015.
1009 Morford, J. L. and Emerson, S.: The geochemistry of redox sensitive trace metals in sediments,
1010 *Geochimica et Cosmochimica Acta*, 63, 1735-1750, 1999.
1011 Nakamura, H., Nishina, A., Liu, Z. J., Tanaka, F., Wimbush, M., and Park, J. H.: Intermediate and
1012 deep water formation in the Okinawa Trough, *Journal of Geophysical Research-Oceans*, 118,
1013 6881-6893, 2013.
1014 Nameroff, T. J., Balistrieri, L. S., and Murray, J. W.: Suboxic trace metal geochemistry in the
1015 Eastern Tropical North Pacific, *Geochimica et Cosmochimica Acta*, 66, 1139-1158, 2002.
1016 Nameroff, T. J., Calvert, S. E., and Murray, J. W.: Glacial-interglacial variability in the eastern
1017 tropical North Pacific oxygen minimum zone recorded by redox-sensitive trace metals,
1018 *Paleoceanography*, 19, PA1010, doi:10.1029/2003PA000912, 2004.
1019 Nishina, A., Nakamura, H., Park, J.-H., Hasegawa, D., Tanaka, Y., Seo, S., and Hibiya, T.: Deep
1020 ventilation in the Okinawa Trough induced by Kerama Gap overflow, *Journal of Geophysical
1021 Research: Oceans*, 121, 6092-6102, 2016.
1022 Ohkushi, K., Hara, N., Ikehara, M., Uchida, M., and Ahagon, N.: Intensification of North Pacific
1023 intermediate water ventilation during the Younger Dryas, *Geo-Mar Lett*, 36, 353-360, 2016.
1024 Ohkushi, K., Itaki, T., and Nemoto, N.: Last Glacial-Holocene change in intermediate-water
1025 ventilation in the Northwestern Pacific, *Quaternary Science Reviews*, 22, 1477-1484, 2003.
1026 Ohkushi, K., Kennett, J. P., Zeleski, C. M., Moffitt, S. E., Hill, T. M., Robert, C., Beaufort, L., and
1027 Behl, R. J.: Quantified intermediate water oxygenation history of the NE Pacific: A new benthic
1028 foraminiferal record from Santa Barbara basin, *Paleoceanography*, 28, 453-467, 2013.
1029 Okazaki, Y., Kimoto, K., Asahi, H., Sato, M., Nakamura, Y., and Harada, N.: Glacial to deglacial
1030 ventilation and productivity changes in the southern Okhotsk Sea, *Palaeogeography
1031 Palaeoclimatology Palaeoecology*, 395, 53-66, 2014.
1032 Okazaki, Y., Sagawa, T., Asahi, H., Horikawa, K., and Onodera, J.: Ventilation changes in the
1033 western North Pacific since the last glacial period, *Climate of the Past*, 8, 17-24, 2012.
1034 Okazaki, Y., Seki, O., Nakatsuka, T., Sakamoto, T., Ikehara, M., and Takahashi, K.: *Cycladophora
1035 davisiana* (Radiolaria) in the Okhotsk Sea: A key for reconstructing glacial ocean conditions,
1036 *Journal of Oceanography*, 62, 639-648, 2006.
1037 Okazaki, Y., Timmermann, A., Menviel, L., Harada, N., Abe-Ouchi, A., Chikamoto, M. O.,
1038 Mouchet, A., and Asahi, H.: Deepwater Formation in the North Pacific During the Last Glacial
1039 Termination, *Science*, 329, 200-204, 2010.
1040 Okumura, Y. M., Deser, C., Hu, A., Timmermann, A., and Xie, S.-P.: North Pacific Climate
1041 Response to Freshwater Forcing in the Subarctic North Atlantic: Oceanic and Atmospheric
1042 Pathways, *Journal of Climate*, 22, 1424-1445, 2009.
1043 Porter, S. C. and Zhisheng, A.: Correlation between climate events in the North Atlantic and China
1044 during the last glaciation, *Nature*, 375, 305-308, 1995.
1045 Praetorius, S. K., Mix, A. C., Walczak, M. H., Wolhowe, M. D., Addison, J. A., and Prahl, F. G.:
1046 North Pacific deglacial hypoxic events linked to abrupt ocean warming, *Nature*, 527, 362-366,
1047 2015.
1048 Qu, T. and Lukas, R.: The Bifurcation of the North Equatorial Current in the Pacific, *Journal of
1049 Physical Oceanography*, 33, 5-18, 2003.

1050 Rühlemann, C., Müller, P. J., and Schneider, R. R.: Organic Carbon and Carbonate as
1051 Paleoproductivity Proxies: Examples from High and Low Productivity Areas of the Tropical
1052 Atlantic. In: Use of Proxies in Paleoceanography: Examples from the South Atlantic, Fischer, G.
1053 and Wefer, G. (Eds.), Springer Berlin Heidelberg, Berlin, Heidelberg, 1999.

1054 Rae, J. W. B., Sarnthein, M., Foster, G. L., Ridgwell, A., Grootes, P. M., and Elliott, T.: Deep
1055 water formation in the North Pacific and deglacial CO₂ rise, *Paleoceanography*, 29, 645-667,
1056 2014.

1057 Reimer, P. J., Bard, E., Bayliss, A., Beck, J. W., Blackwell, P. G., Bronk Ramsey, C., Buck, C. E.,
1058 Cheng, H., Edwards, R. L., Friedrich, M., Grootes, P. M., Guilderson, T. P., Haflidason, H., Hajdas,
1059 I., Hatté, C., Heaton, T. J., Hoffmann, D. L., Hogg, A. G., Hughen, K. A., Kaiser, K. F., Kromer,
1060 B., Manning, S. W., Niu, M., Reimer, R. W., Richards, D. A., Scott, E. M., Southon, J. R., Staff, R.
1061 A., Turney, C. S. M., and van der Plicht, J.: IntCal13 and Marine13 Radiocarbon Age Calibration
1062 Curves 0–50,000 Years cal BP, *Radiocarbon*, 55, 1869-1887, 2013.

1063 Rella, S. F., Tada, R., Nagashima, K., Ikehara, M., Itaki, T., Ohkushi, K., Sakamoto, T., Harada, N.,
1064 and Uchida, M.: Abrupt changes of intermediate water properties on the northeastern slope of the
1065 Bering Sea during the last glacial and deglacial period, *Paleoceanography*, 27, PA3203,
1066 doi:3210.1029/2011pa002205, 2012.

1067 Riethdorf, J.-R., Max, L., Nuernberg, D., Lembke-Jene, L., and Tiedemann, R.: Deglacial
1068 development of (sub) sea surface temperature and salinity in the subarctic northwest Pacific:
1069 Implications for upper-ocean stratification, *Paleoceanography*, 28, doi:10.1002/palo.20014, 2013.

1070 Riethdorf, J.-R., Thibodeau, B., Ikehara, M., Nürnberg, D., Max, L., Tiedemann, R., and
1071 Yokoyama, Y.: Surface nitrate utilization in the Bering sea since 180ka BP: Insight from
1072 sedimentary nitrogen isotopes, *Deep Sea Research Part II: Topical Studies in Oceanography*,
1073 125-126, 163-176, 2016.

1074 Rippert, N., Max, L., Mackensen, A., Cacho, I., Povea, P., and Tiedemann, R.: Alternating
1075 Influence of Northern Versus Southern-Sourced Water Masses on the Equatorial Pacific
1076 Subthermocline During the Past 240 ka, *Paleoceanography*, 32, 1256-1274, 2017.

1077 Rodríguez-Sanz, L., Mortyn, P. G., Herguera, J. C., and Zahn, R.: Hydrographic changes in the
1078 tropical and extratropical Pacific during the last deglaciation, *Paleoceanography*, 28, 529-538,
1079 2013.

1080 Saenko, O. A., Schmittner, A., and Weaver, A. J.: The Atlantic-Pacific seesaw, *Journal of Climate*,
1081 17, 2033-2038, 2004.

1082 Sagawa, T. and Ikehara, K.: Intermediate water ventilation change in the subarctic northwest
1083 Pacific during the last deglaciation, *Geophysical Research Letters*, 35, 5, doi:
1084 10.1029/2008gl035133, 2008.

1085 Scott, C. and Lyons, T. W.: Contrasting molybdenum cycling and isotopic properties in euxinic
1086 versus non-euxinic sediments and sedimentary rocks: Refining the paleoproxies, *Chemical
1087 Geology*, 324–325, 19-27, 2012.

1088 Scott, C., Lyons, T. W., Bekker, A., Shen, Y., Poulton, S. W., Chu, X., and Anbar, A. D.: Tracing
1089 the stepwise oxygenation of the Proterozoic ocean, *Nature*, 452, 456-459, 2008.

1090 Shao, H., Yang, S., Cai, F., Li, C., Liang, J., Li, Q., Hyun, S., Kao, S.-J., Dou, Y., Hu, B., Dong, G.,
1091 and Wang, F.: Sources and burial of organic carbon in the middle Okinawa Trough during late
1092 Quaternary paleoenvironmental change, *Deep Sea Research Part I: Oceanographic Research
1093 Papers*, 118, 46-56, 2016.

1094 Shcherbina, A. Y., Talley, L. D., and Rudnick, D. L.: Direct observations of North Pacific
1095 ventilation: Brine rejection in the Okhotsk Sea, *Science*, 302, 1952-1955, 2003.

1096 Shi, X., Wu, Y., Zou, J., Liu, Y., Ge, S., Zhao, M., Liu, J., Zhu, A., Meng, X., Yao, Z., and Han, Y.:
1097 Multiproxy reconstruction for Kuroshio responses to northern hemispheric oceanic climate and the
1098 Asian Monsoon since Marine Isotope Stage 5.1 (~88 ka), *Climate of the Past*, 10, 1735-1750,
1099 2014.

1100 Shibahara, A., Ohkushi, K., Kennett, J. P., and Ikehara, K.: Late Quaternary changes in
1101 intermediate water oxygenation and oxygen minimum zone, northern Japan: A benthic
1102 foraminiferal perspective, *Paleoceanography*, 22, PA3213, doi:3210.1029/2005pa001234, 2007.

1103 Shimmield, G. B. and Price, N. B.: The behaviour of molybdenum and manganese during early
1104 sediment diagenesis — offshore Baja California, Mexico, *Marine Chemistry*, 19, 261-280, 1986.

1105 Sibuet, J. C., Letouzey, J., Barbier, F., Charvet, J., Foucher, J. P., Hilde, T. W. C., Kimura, M.,
1106 Chiao, L.-Y., Marsset, B., Muller, C., and Stéphan, J. F.: Back Arc Extension in the Okinawa
1107 Trough, *Journal of Geophysical Research: Solid Earth*, 92, 14041-14063, 1987.

1108 Sigman, D. M. and Boyle, E. A.: Glacial/interglacial variations in atmospheric carbon dioxide,
1109 *Nature*, 407, 859-869, 2000.

1110 Spratt, R. M. and Lisiecki, L. E.: A Late Pleistocene sea level stack, *Clim. Past*, 12, 1079-1092,
1111 2016.

1112 Sun, Y., Clemens, S. C., Morrill, C., Lin, X., Wang, X., and An, Z.: Influence of Atlantic
1113 meridional overturning circulation on the East Asian winter monsoon, *Nature Geosci*, 5, 46-49,
1114 2012.

1115 Sun, Y. B., Oppo, D. W., Xiang, R., Liu, W. G., and Gao, S.: Last deglaciation in the Okinawa
1116 Trough: Subtropical northwest Pacific link to Northern Hemisphere and tropical climate,
1117 *Paleoceanography*, 20, PA4005, doi:4010.1029/2004pa001061, 2005.

1118 Sundby, B., Martinez, P., and Gobeil, C.: Comparative geochemistry of cadmium, rhenium,
1119 uranium, and molybdenum in continental margin sediments, *Geochimica et Cosmochimica Acta*,
1120 68, 2485-2493, 2004.

1121 Talley, L. D.: Distribution forantion of North Pacific Intermediate water, *Journal of Physical*
1122 *Oceanography*, 23, 517-537, 1993.

1123 Talley, L. D.: Hydrographic Atlas of the World Ocean Circulation Experiment (WOCE). In:
1124 Volume 2: Pacific Ocean, Sparrow, M., Chapman, P., and Gould, J. (Eds.), International WOCE
1125 Project Office, Southampton, UK, 2007.

1126 Tribovillard, N., Algeo, T. J., Lyons, T., and Riboulleau, A.: Trace metals as paleoredox and
1127 paleoproductivity proxies: An update, *Chemical Geology*, 232, 12-32, 2006.

1128 Ujiié, H. and Ujiié, Y.: Late Quaternary course changes of the Kuroshio Current in the Ryukyu Arc
1129 region, northwestern Pacific Ocean, *Marine Micropaleontology*, 37, 23-40, 1999.

1130 Ujiié, Y., Asahi, H., Sagawa, T., and Bassinot, F.: Evolution of the North Pacific Subtropical Gyre
1131 during the past 190 kyr through the interaction of the Kuroshio Current with the surface and
1132 intermediate waters, *Paleoceanography*, 31, 1498-1513, 2016.

1133 Ujiié, Y., Ujiié, H., Taira, A., Nakamura, T., and Oguri, K.: Spatial and temporal variability of
1134 surface water in the Kuroshio source region, Pacific Ocean, over the past 21,000 years: evidence
1135 from planktonic foraminifera, *Marine Micropaleontology*, 49, 335-364, 2003.

1136 Vorliceck, T. P. and Helz, G. R.: Catalysis by mineral surfaces: Implications for Mo geochemistry
1137 in anoxic environments, *Geochimica et Cosmochimica Acta*, 66, 3679-3692, 2002.

1138 Wahyudi and Minagawa, M.: Response of benthic foraminifera to organic carbon accumulation
1139 rates in the Okinawa Trough, *Journal of Oceanography*, 53, 411-420, 1997.

1140 Wan, S. and Jian, Z.: Deep water exchanges between the South China Sea and the Pacific since the
1141 last glacial period, *Paleoceanography*, 29, 1162-1178, 2014.

1142 Wang, Y., Cheng, H., Edwards, R. L., He, Y., Kong, X., An, Z., Wu, J., Kelly, M. J., Dykoski, C.
1143 A., and Li, X.: The Holocene Asian Monsoon: Links to Solar Changes and North Atlantic Climate,
1144 *Science*, 308, 854-857, 2005.

1145 Wu, Y., Cheng, Z., and Shi, X.: Stratigraphic and carbonate sediment characteristics of Core CSH1
1146 from the northern Okinawa Trough, *Advances in Marine Science*, 22, 163-169, 2004 (in Chinese
1147 with English Abstract).

1148 Wu, Y., Shi, X., Zou, J., Cheng, Z., Wang, K., Ge, S., and Shi, F.: Benthic foraminiferal $\delta^{13}\text{C}$
1149 minimum events in the southeastern Okhotsk Sea over the last 180ka, *Chinese Science Bulletin*,
1150 59, 3066-3074, 2014.

1151 You, Y. Z.: The pathway and circulation of North Pacific Intermediate Water, *Geophysical*
1152 *Research Letters*, 30, doi:10.1029/2003gl018561, 2003.

1153 You, Y. Z., Suginozawa, N., Fukasawa, M., Yasuda, I., Kaneko, I., Yoritaka, H., and Kawamiya, M.:
1154 Roles of the Okhotsk Sea and Gulf of Alaska in forming the North Pacific Intermediate Water,
1155 *Journal of Geophysical Research-Oceans*, 105, 3253-3280, 2000.

1156 You, Y. Z., Suginozawa, N., Fukasawa, M., Yoritaka, H., Mizuno, K., Kashino, Y., and Hartoyo, D.:
1157 Transport of North Pacific Intermediate Water across Japanese WOCE sections, *Journal of*
1158 *Geophysical Research-Oceans*, 108, doi: 10.1029/2002jc001662, 2003.

1159 Yu, H., Liu, Z. X., Berne, S., Jia, G. D., Xiong, Y. Q., Dickens, G. R., Wei, G. J., Shi, X. F., Liu, J.
1160 P., and Chen, F. J.: Variations in temperature and salinity of the surface water above the middle
1161 Okinawa Trough during the past 37 kyr, *Palaeogeography Palaeoclimatology Palaeoecology*, 281,
1162 154-164, 2009.

1163 Zhang, X., Knorr, G., Lohmann, G., and Barker, S.: Abrupt North Atlantic circulation changes in
1164 response to gradual CO₂ forcing in a glacial climate state, *Nature Geoscience*, 10, 518-524, 2017.

1165 Zhao, D., Wan, S., Toucanne, S., Clift, P. D., Tada, R., Révillon, S., Kubota, Y., Zheng, X., Yu, Z.,
1166 Huang, J., Jiang, H., Xu, Z., Shi, X., and Li, A.: Distinct control mechanism of fine-grained
1167 sediments from Yellow River and Kyushu supply in the northern Okinawa Trough since the last
1168 glacial, *Geochemistry, Geophysics, Geosystems*, 18, 2949-2969, 2017.

1169 Zheng, X., Kao, S., Chen, Z., Menviel, L., Chen, H., Du, Y., Wan, S., Yan, H., Liu, Z., Zheng, L.,
1170 Wang, S., Li, D., and Zhang, X.: Deepwater circulation variation in the South China Sea since the
1171 Last Glacial Maximum, *Geophysical Research Letters*, 43, 8590-8599, 2016.

1172 Zheng, Y., Anderson, R., van Geen, A., and Fleisher, M.: Remobilization of authigenic uranium in
1173 marine sediments by bioturbation, *Geochimica et Cosmochimica Acta*, 66, 1759-1772, 2002.

1174 Zheng, Y., Anderson, R., van Geen, A., and Kuwabara, J.: Authigenic molybdenum formation in
1175 marine sediments: a link to pore water sulfide in the Santa Barbara Basin, *Geochimica et*
1176 *Cosmochimica Acta*, 64, 4165-4178, 2000.

1177 Zhu, A., Shi, X., Zou, J., Wu, Y., Zhang, H., and Bai, Y.: Sediment Provenance and Fluxes in the
1178 Northern Okinawa Trough During the last 88ka, *Marine Geology & Quaternary Geology*, 35, 1-8 ,
1179 2015 (in Chinese with English Abstract).

1180 Zou, J., Shi, X., Liu, Y., Liu, J., Selvaraj, K., and Kao, S.-J.: Reconstruction of environmental
1181 changes using a multi-proxy approach in the Ulleung Basin (Sea of Japan) over the last 48 ka,

1182 Journal of Quaternary Science, 27, 891-900, 2012.

1183

1184 **Captions**

1185 **Table 1.** Locations of different sediment core records and their source references
1186 discussed in the text.

1187

1188 **Table 2.** Age control points adopted between planktic foraminifera species
1189 *Globigerinoides ruber* $\delta^{18}\text{O}$ of Core CSH1 and Chinese stalagmite $\delta^{18}\text{O}$ (Cheng et al.,
1190 2016) for tuning the age model between 10 ka and 60 ka in this study. A linear
1191 interpolation was assumed between age control points.

1192

1193 **Figure 1.** (a) Spatial distribution of dissolved oxygen content at 700 m water depth in
1194 the North Pacific. Black arrows denote simplified Kuroshio and Oyashio circulations
1195 and North Pacific Intermediate Water (NPIW) in the North Pacific. The red thick
1196 dashed line indicates transformation of Okhotsk Sea Intermediate Water (OSIW) by
1197 cabbeling the subtropical NPIW along the subarctic-tropical frontal zone (You, 2003).
1198 The light brown solid line with arrow indicates the spreading path of subtropical
1199 NPIW from northeast North Pacific southward toward the low-latitude northwest
1200 North Pacific (You, 2003). Yellow solid lines with arrow represent two passages
1201 through which NPIW enter into the Okinawa Trough. This figure was created with
1202 Ocean Data View (odv.awi.de). (b) Location of sediment core CSH1 investigated in
1203 this study (red diamond). Also shown are locations of sediment cores PN-3, E017, 255
1204 and MD012404 investigated previously from the Okinawa Trough, GH08-2004 from
1205 the East of Ryukyu Island, GH02-1030 off the east of Japan, PC-23A from the Bering
1206 Sea and ODP Site 1017 from the northeastern Pacific. Letters A to E represent the
1207 sediment cores from and near the OT. The detailed information for these cores is
1208 shown in Table 1.

1209

1210 **Figure 2.** Spatial distribution of sea surface salinity in the East China Sea. (a) summer
1211 (July to September); (b) winter (January to March). Lower sea surface salinity in
1212 summer relative to that of winter indicates strong effects of summer East Asian
1213 Monsoon.

1214

1215 **Figure 3.** (a) Lithology and oxygen isotope ($\delta^{18}\text{O}$) profile of planktic foraminifera
1216 species *Globigerinoides ruber* (*G.ruber*) in core CSH1. (b) Plot of ages versus depth
1217 for core CSH1. Three known ash layers are indicated by solid red rectangles. (c) Time
1218 series of linear sedimentation rate (LSR) from core CSH1. (d) Comparison of age
1219 model of core CSH1 with Chinese Stalagmite composite $\delta^{18}\text{O}$ curve of (Cheng et al.,
1220 2016). Tie points for CSH1 core chronology (Table 2) in Figures 3c and 3d are
1221 designated by colored crosses.

1222

1223 **Figure 4.** Age versus (a) CaCO_3 concentration, (b) Total nitrogen (TN) concentration,
1224 (c) Total organic carbon (TOC) concentration, (d) C/N molar ratio, (e) linear
1225 sedimentation rate (LSR), (f) Al concentration, (g) Mn concentration, (h) Mo/Mn ratio,
1226 (i) Mo concentration, (j) excess Mo concentration, (k) U concentration and (l) excess
1227 U concentration and (m) $(\text{Mo}/\text{U})_{\text{excess}}$ ratio in core CSH1. Light gray and dark gray
1228 vertical bars indicate different sediment intervals in core CSH1. 8.2 ka, PB, YD, B/A,
1229 HS1, LGM and HS2 refer to 8,200 year cold event, Preboreal, Younger Dryas, Bölling
1230 - Alleröd, Heinrich Stadial 1, Last Glacial Maximum and Heinrich Stadial 2,
1231 respectively, which were identified in core CSH1. Blue solid diamonds in Figure 4m
1232 indicate the age control points.

1233

1234 **Figure 5.** Scatter plots of $\text{Mo}_{\text{excess}}$ vs Mn concentrations and U_{excess} concentration vs
1235 Mo/Mn ratio at different time intervals in core CSH1. A various correlation is present
1236 in core CSH1 at different time intervals, which shows their complicated geochemical
1237 behaviors (Figs.5a and 5b). Strong positive correlation between Mo/Mn ratio and
1238 U_{excess} concentration (Fig.5c) suggest that Mo/Mn ratio is a reliable proxy to track
1239 sedimentary redox conditions in the geological past.

1240

1241 **Figure 6.** Proxy-related reconstructions of mid-depth sedimentary oxygenation at site
1242 CSH1 (this study) compared with oxygenation records from other locations of the
1243 North Pacific and published climatic and environmental records from the Okinawa

1244 Trough. From top to bottom: (a) CaCO₃ concentration, (b) U_{excess} concentration, (c)
1245 Mo/Mn ratio, and (d) sea surface temperature (SST) (Shi et al., 2014), (e) abundance
1246 of *P.obliquiloculata* in core CSH1 (Shi et al., 2014), (f) bulk sedimentary organic
1247 matter δ¹⁵N in core MD01-2404 (Kao et al., 2008), (g) δ¹³C of epibenthic
1248 foraminiferal *C.wuellerstorfi* in core PN-3 (Wahyudi and Minagawa, 1997), (h)
1249 relative abundance of *B. aculeata* (hypoxia-indicating species) and (i) *C.hyalinea*
1250 (oxygen-rich indicating species) (Li et al., 2005), (j) dysoxic taxa (%) in core ODP
1251 167-1017 in the northeastern Pacific (Cannariato and Kennett, 1999) and (k) δ¹³C of
1252 benthic foraminiferal *Uvigerina akitaensis* in core PC23A in the Bering Sea (Rella
1253 et al., 2012). Light gray and dark gray vertical bars are the same as those in Figure 4.

1254

1255 **Figure 7.** Proxy records favoring the existence of out-of-phase connections between
1256 the subtropical North Pacific and North Atlantic during the last deglaciation and
1257 enhanced carbon storage at mid-depth waters. (a) U_{excess} concentration in core CSH1;
1258 (b) Mo/Mn ratio in core CSH1; (c) benthic δ¹³C record in core PC-23A in the Bering
1259 Sea (Rella et al., 2012); (d) Indicator of strength of Atlantic Meridional Ocean
1260 Circulation (²³¹Pa/²³⁰Th) (Böhm et al., 2015; McManus et al., 2004); (e) Atmospheric
1261 CO₂ concentration (Marcott et al., 2014). Light gray and dark gray vertical bars are
1262 the same as those in Figure 4.

1263

Table 1

Label in Figure 1b	Station	Latitude (°N)	Longitude (°E)	Water depth (m)	Area	Reference
	CSH1	31.23	128.72	703	Okinawa Trough	this study
A	PN-3	28.10	127.34	1058	Okinawa Trough	Wahyudi and Minagawa, (1997)
B	MD012404	26.65	125.81	1397	Okinawa Trough	Kao et al., (2008)
C	E017	26.57	126.02	1826	Okinawa Trough	Li et al., (2005)
D	255	25.20	123.12	1575	Okinawa Trough	Jian et al., (1996)
E	GH08-2004	26.21	127.09	1166	East of Ryukyu Island	Kubota et al. (2015)
	GH02-1030	42.23	144.21	1212	Off Japan	Sagawa and Ikehara, (2008)
	PC-23A	60.16	179.46	1002	Bering Sea	Rella et al.,(2012)
	ODP Site1017	34.54	239.11	955	NE Pacific	Cannariato and Kennett, (1999)

1 Table 2

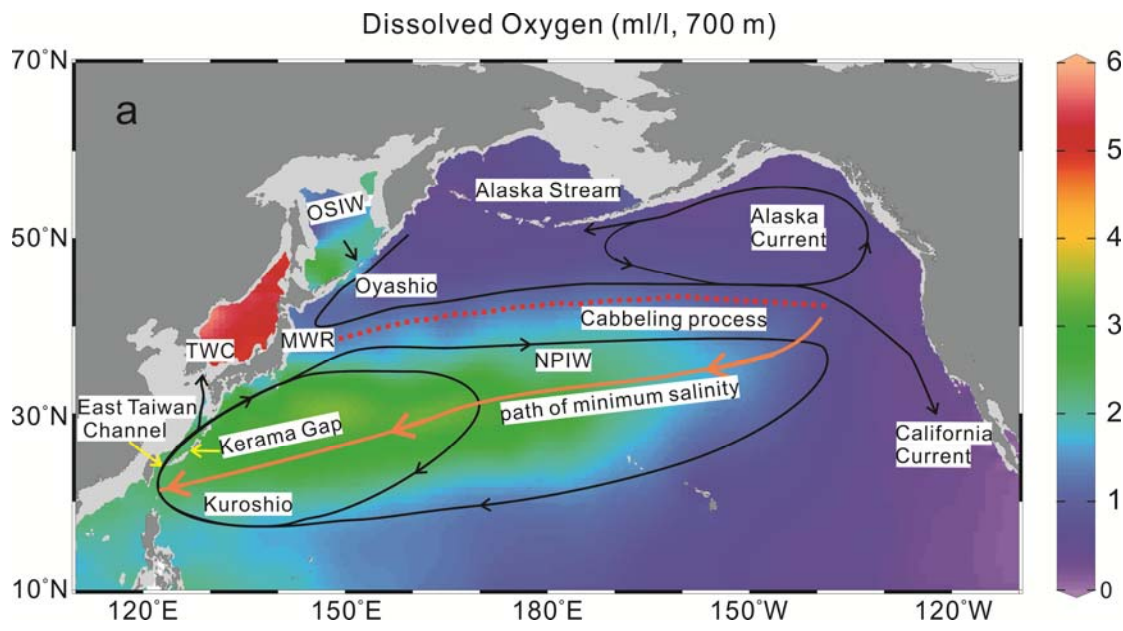
2

Depth(cm)	AMS ¹⁴ C (yr)	Error (yr)	Calibrated Age (yr)	Tie Point Type	LSR (cm/ka)	Source
10	3420	±35	3296	¹⁴ C		Shi et al., (2014)
106	7060	± 40	7545	¹⁴ C	22.59	Shi et al., (2014)
218			12352	Stalagmite, YD	23.30	This study
322			16029	Stalagmite, H1	28.28	This study
362			19838	Stalagmite	10.50	This study
506			24163	Stalagmite, H2	33.29	This study
698			28963	Stalagmite, DO4	40.00	This study
834			32442	Stalagmite, DO5	39.09	This study
938			37526	Stalagmite, DO8	20.46	This study
978			39468	Stalagmite, H4	20.60	This study
1058			46151	Stalagmite, DO12	11.97	This study
1122			49432	Stalagmite, DO13	19.51	This study
1242			52831	Stalagmite, DO14	35.30	This study
1282			57241	Stalagmite, DO16	9.07	This study
1346			61007	Stalagmite, H6	16.99	This study
1530		±2590	73910	MIS4/5	14.26	Shi et al., (2014)
1610		±3580	79250	MIS 5.1	14.98	Shi et al., (2014)

3

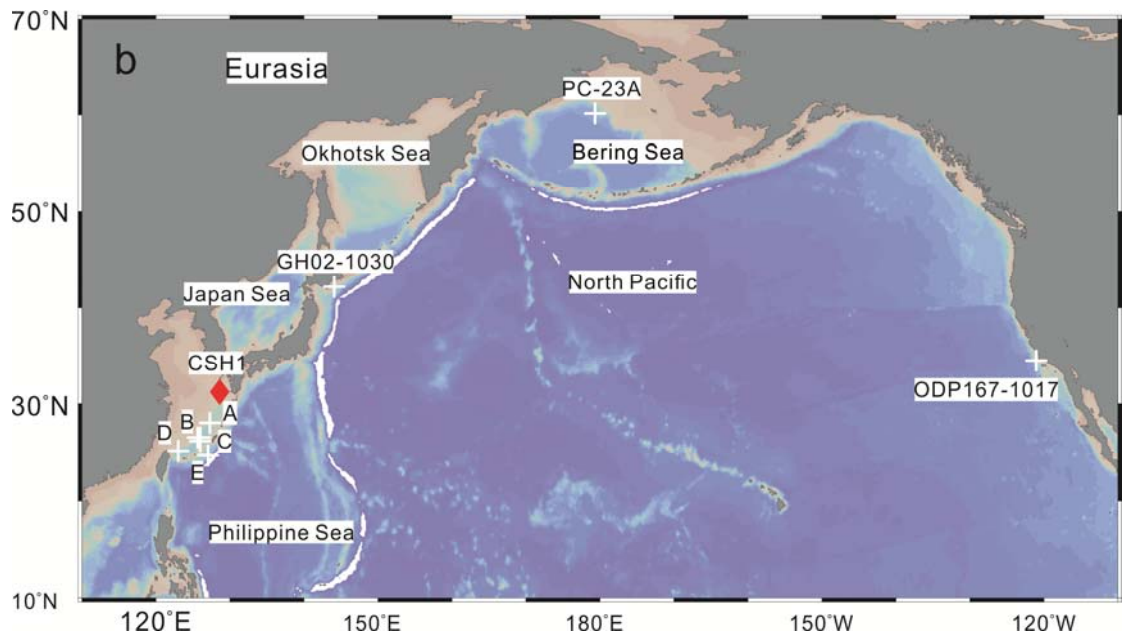
4

5 Fig.1



6

7

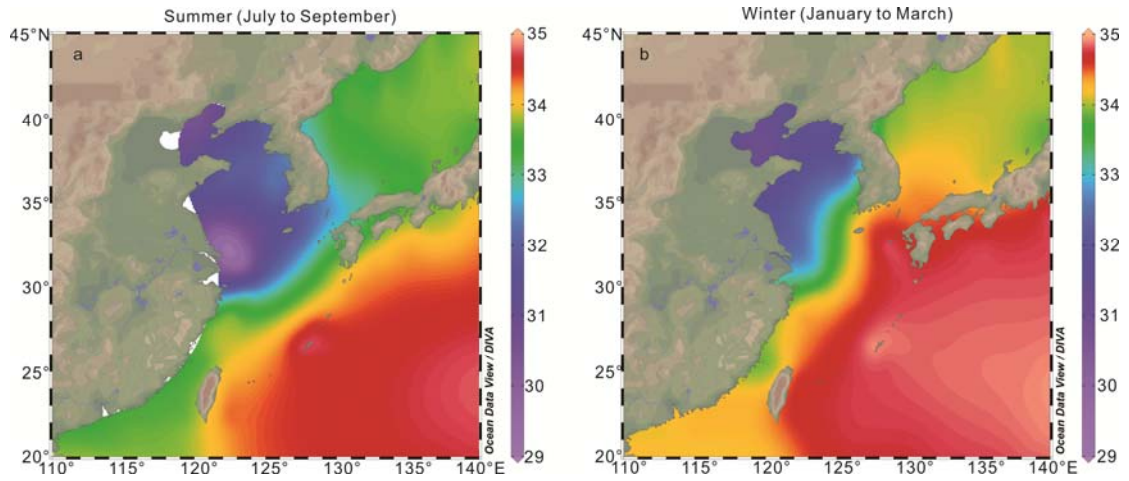


8

9

10

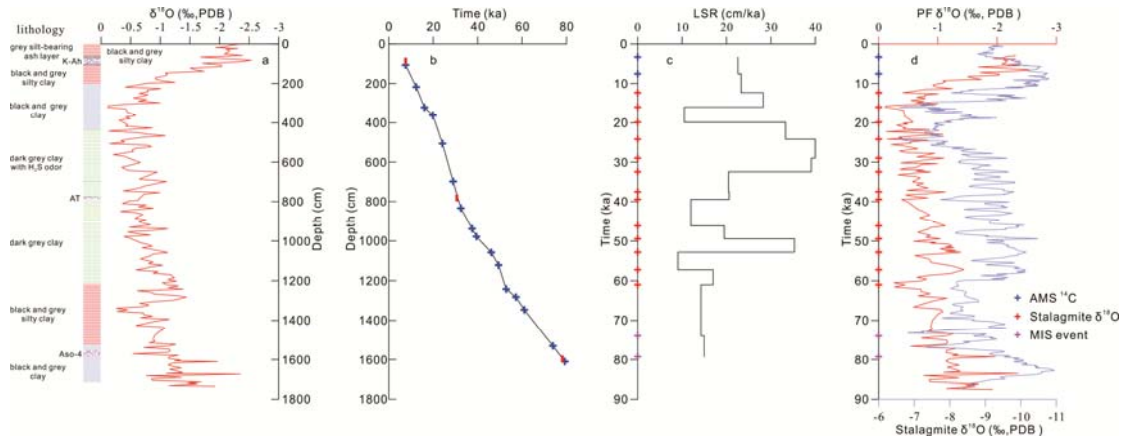
11 Fig.2



12

13

14 Fig.3

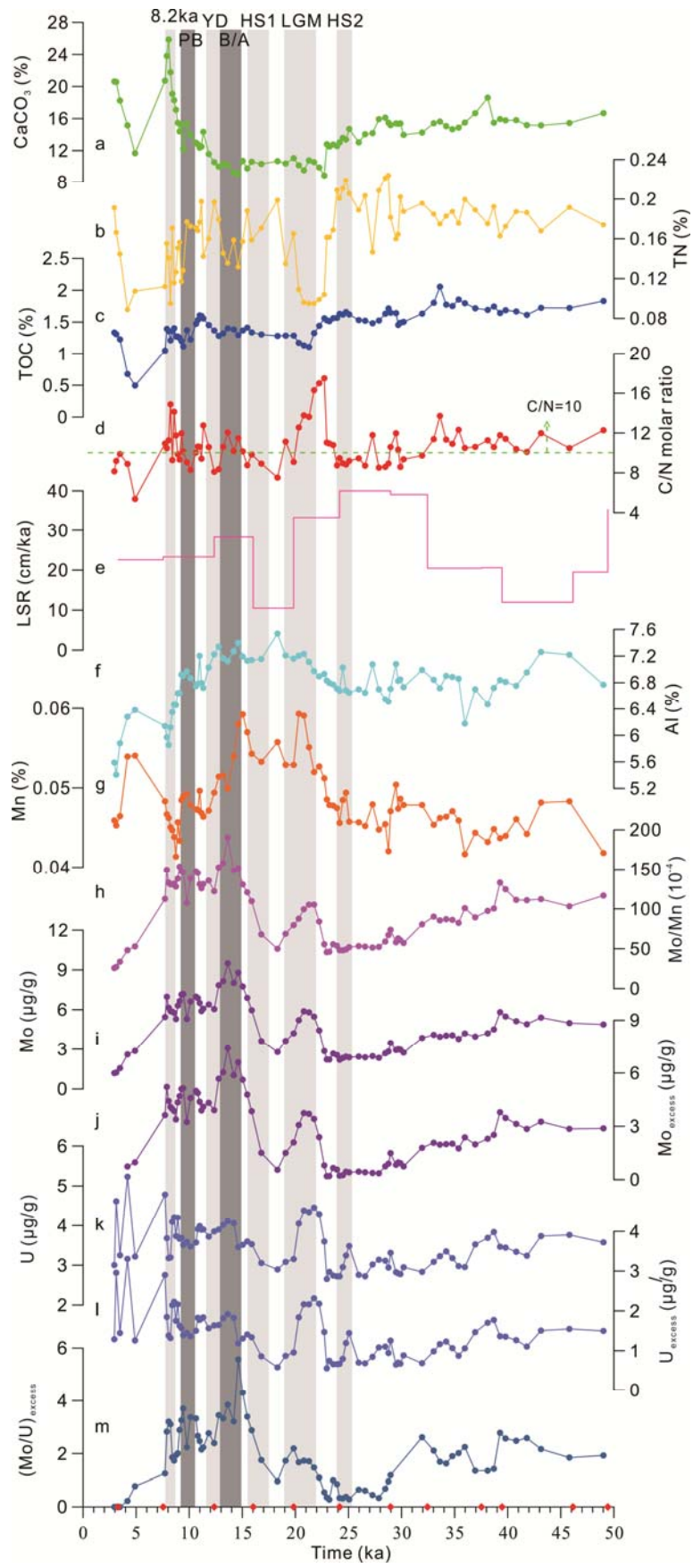


15

16

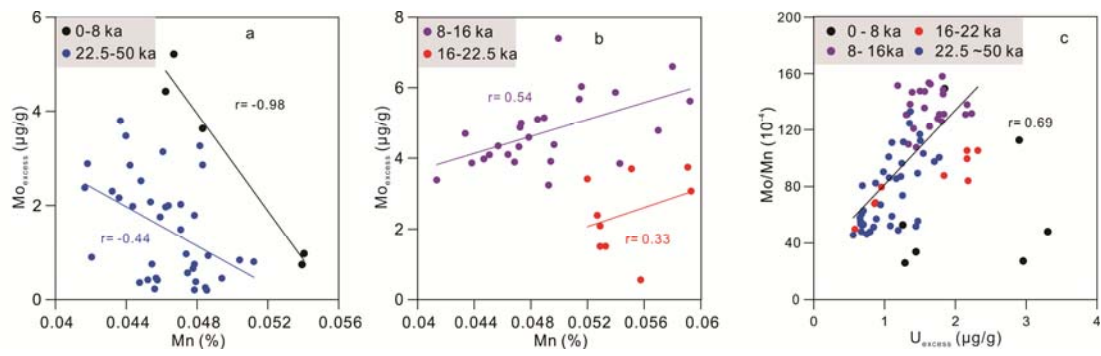
17

18 Fig.4



20 Fig.5

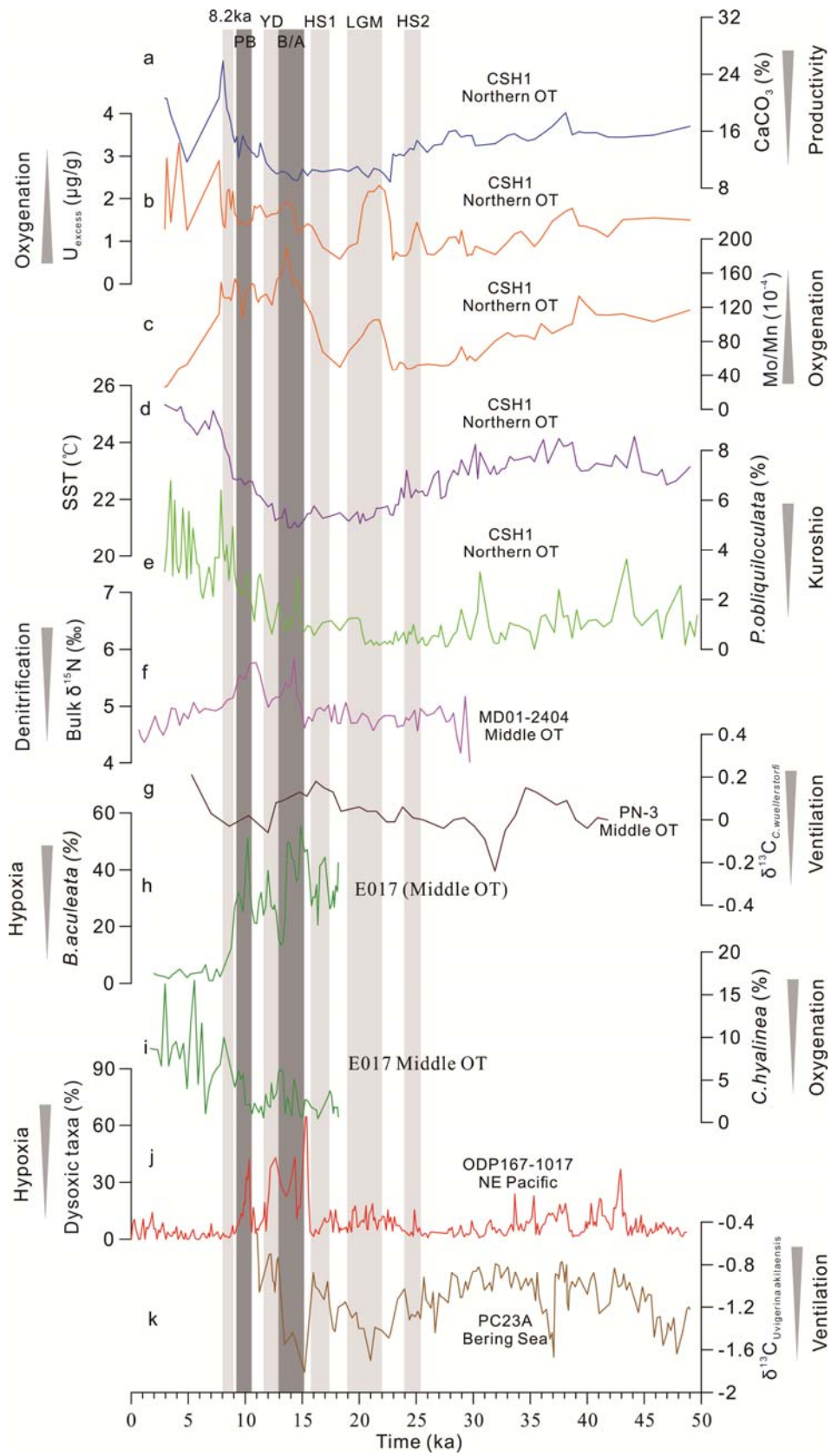
21



22

23

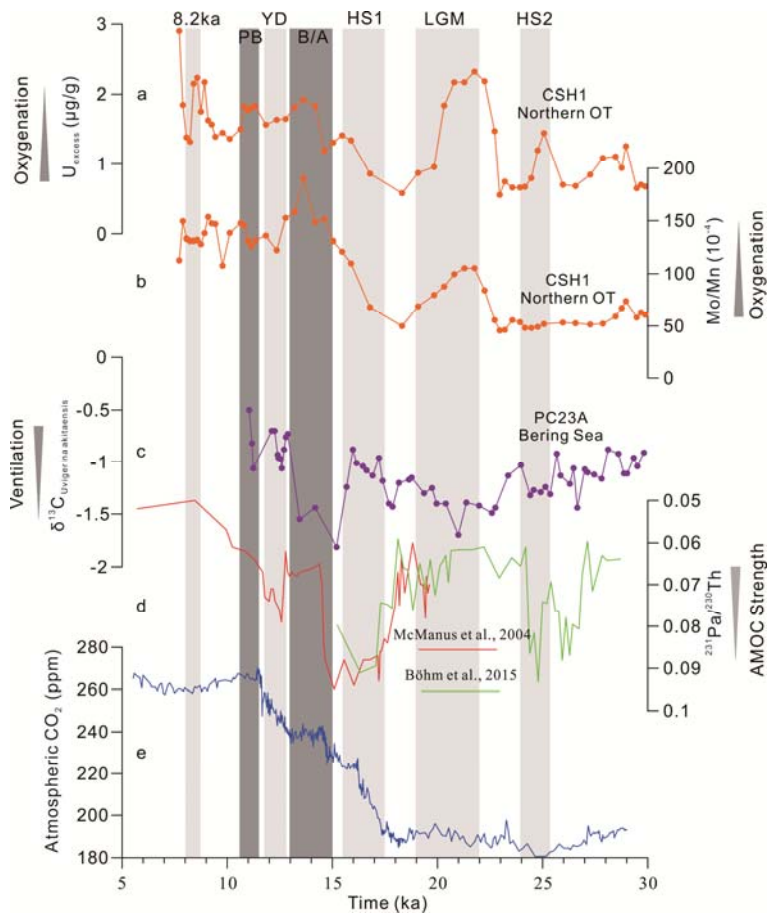
24 Fig.6



25

26

27 Fig.7



28

29